

# Perforated 3D concrete printing

Controlling the variations in perforations of a 3D concrete printed texture

Broothaers Robbe

Thesis voorgedragen tot het behalen  
van de graad van Master of Science  
in de ingenieurswetenschappen:  
architectuur

**Promotoren:**

Prof. dr. ir. Andrew Vande Moere  
Prof. dr. ir. Stefan Peters

Academiejaar 2022 – 2023



# Perforated 3D concrete printing

Controlling the variations in perforations of a 3D concrete printed texture

Broothaers Robbe

Thesis voorgedragen tot het behalen  
van de graad van Master of Science  
in de ingenieurswetenschappen:  
architectuur

**Promotoren:**

Prof. dr. ir. Andrew Vande Moere  
Prof. dr. ir. Stefan Peters

**Evaluatoren:**

Prof. Herman Bruyninckx  
Ir. Iremnur Tokac

**Begeleider:**

Ir. Robert Schmid

© Copyright KU Leuven

Without written permission of the supervisors and the author it is forbidden to reproduce or adapt in any form or by any means any part of this publication. Requests for obtaining the right to reproduce or utilize parts of this publication should be addressed to Faculteit Ingenieurswetenschappen, Kasteelpark Arenberg 1 bus 2200, B-3001 Heverlee, +32-16-321350.

A written permission of the supervisors is also required to use the methods, products, schematics and programmes described in this work for industrial or commercial use, and for submitting this publication in scientific contests.

Zonder voorafgaande schriftelijke toestemming van zowel de promotoren als de auteur is overnemen, kopiëren, gebruiken of realiseren van deze uitgave of gedeelten ervan verboden. Voor aanvragen tot of informatie i.v.m. het overnemen en/of gebruik en/of realisatie van gedeelten uit deze publicatie, wend u tot Faculteit Ingenieurswetenschappen, Kasteelpark Arenberg 1 bus 2200, B-3001 Heverlee, +32-16-321350.

Voorafgaande schriftelijke toestemming van de promotoren is eveneens vereist voor het aanwenden van de in deze masterproef beschreven (originele) methoden, producten, schakelingen en programma's voor industrieel of commercieel nut en voor de inzending van deze publicatie ter deelname aan wetenschappelijke prijzen of wedstrijden.

# ABSTRACT

Deze thesis presenteert een nieuwe aanpak voor het creëren van een geperforeerd gevelpaneel met behulp van 3D-betonprinttechnologie. Het gebruik van perforaties in de gevel maakt zonwering mogelijk en zorgt tegelijkertijd voor voldoende daglicht binnenshuis. Met de toenemende populariteit van digitale bouwmethoden is de constructie van geperforeerde gevels toegankelijker geworden, 3D-betonprinten is een veelbelovende methode voor maatwerk op grote schaal in deze categorie. Echter heeft deze nog niet bewezen efficiënt te zijn voor het creëren van perforaties. In deze scriptie wordt de geschiktheid van een 3D-betonprinter om een geperforeerd gevelpaneel te creëren geanalyseerd. Verschillende toolpath-technieken voor het creëren van perforaties worden getest door middel van praktische testprints. De meest veelbelovende toolpath-techniek wordt verder onderzocht om het algoritme voor het creëren van de perforaties te optimaliseren. Verwachte resultaten van dit onderzoek zijn onder andere een gevalideerd algoritme voor het creëren en regelen van perforaties met een 3D-betonprinter, met de mogelijkheid om een ruw oppervlaktetextuur te creëren, alsook variaties en patronen met de perforaties te creëren. Daarnaast zal een set ontwerpcriteria worden vastgesteld om specifieke esthetische en functionele resultaten te behalen. Dit gaat samen met een beter begrip van de beperkingen en uitdagingen van de technologie voor architecturale toepassingen, specifiek voor geperforeerde panelen. Deze scriptie zal een beter begrip bieden van het potentieel en de beperkingen van de technologie voor architecturale toepassingen, met name gericht op het creëren van geperforeerde panelen.



# ABSTRACT

This thesis presents a novel approach to fabricate a perforated façade panel using 3D concrete printing technology. The use of perforations in a façade allows for effective solar control, while at the same time providing adequate daylight indoors. With the increasing popularity of digital construction methods, the fabrication of perforated facades has become more accessible. 3D concrete printing is one of these digital construction methods. In this thesis, the suitability of a 3D concrete printing for creating a perforated panel is analysed. Various toolpath techniques for creating perforations are tested through practical test prints. The most promising toolpath technique, which will further be called the *Greek Key Pattern*, is further explored to optimize the algorithm for fabricating the perforations. The outcomes of this research include a validated algorithm for fabricating and controlling perforations with a 3D concrete printer, with the possibility of creating a rough expressive surface texture, and variations with the perforations. Additionally, a set of design criteria is established for controlling specific aesthetic and functional outcomes, along with a better understanding of the limitations and challenges of the technology for architectural application, more specific perforated panels. This research contributes to the growing field of 3D concrete printing and introduces a new way of fabricating perforated panels by introducing the *Greek Key Pattern*, offering architects and designers a new form language for perforated panels.



# DANKWOORD

Het schrijven van deze thesis heeft een integrale rol gespeeld in mijn masterstudies. Het uitvoeren van dit onderzoek, in combinatie met mijn resterende cursussen en mijn Erasmus+ uitwisseling, binnen één jaar tijd bracht talrijke uitdagingen met zich mee. Desondanks ben ik dankbaar voor de enorme steun en begeleiding die ik gedurende deze reis ontvangen heb van verschillende personen.

Allereerst wil ik graag mijn dank uitspreken aan allen die mij hebben geholpen gedurende mijn tijd in Graz, Oostenrijk. Ik ben hier in het bijzonder zeer dankbaar aan mijn co-promotor prof. Stefan Peters, voor zijn ondersteuning en begeleiding gedurende mijn semester aan *TU Graz*. Ook ben ik ontzettend dankbaar aan ir. Robert Schmid die mij heeft begeleid. Zijn expertise op het gebied van 3D-betonprinten en inbreng van ideeën hebben aanzienlijk bijgedragen aan dit onderzoek. Daarnaast wil ik Alexander Dumps bedanken voor zijn hulp en ondersteuning tijdens de tests met de beton printer.

Verder toon ik graag mijn appreciatie jegens *TU Graz* voor de mogelijkheid die ze mij hebben geboden om een semester aan hun instelling door te brengen. Meer specifiek aan het *Institute of Structural Design* dat mij toegang heeft gegeven tot hun innovatieve *robot faciliteit*, waar de BauMinator 3D-betonprinter staat opgesteld. De middelen en ondersteuning die door het instituut zijn geboden hebben een cruciale rol gespeeld in de succesvolle uitvoering van dit onderzoek.

Verder wil ik prof. Vande Moere, mijn begeleider aan *KU Leuven* bedanken voor zijn begeleiding en ondersteuning gedurende het tweede semester. Zijn expertise en feedback hebben bijgedragen aan de ontwikkeling en verfijning van deze scriptie.

Tot slot ben ik mijn vriendin enorm dankbaar, voor haar constante morele steun gedurende dit uitdagende jaar en voor haar hulp bij het proeflezen van mijn conceptscriptie. Haar aanmoediging en geloof in mijn capaciteiten hebben mij gedurende deze studie op de been gehouden.

Zonder de gezamenlijke hulp en bijdragen van de genoemde personen en instellingen zou deze scriptie niet mogelijk zijn geweest. Ik ben zeer dankbaar voor hun begeleiding, aanmoediging en geloof in mijn capaciteiten.



# ACKNOWLEDGEMENT

Writing this thesis has played an integral role in my master's studies. Making this research, alongside my remaining coursework and participation in the Erasmus+ exchange program, within a single year presented numerous challenges. However, I am grateful for receiving tremendous support and guidance from various individuals along this journey.

First of all, I would like to gratefully thank all those who have helped me during my time in Graz, Austria. I am especially grateful to my co-supervisor, prof. Stefan Peters, for his support and guidance throughout my time at *TU Graz*. I am also obliged to assistant-supervisor ir. Robert Schmid, whose expertise in 3D concrete printing and idea development greatly contributed to this research. Additionally, I would like to thank Alexander Dumps for his help and assistance during the practical tests with the concrete printer.

I am deeply thankful to *TU Graz* for providing me with the opportunity to spend a semester at their institution, and more specifically the *institute of structural design* granting me access to their state-of-the-art *processing robot facility*, housing the BauMinator 3D concrete printer. The resources and support offered by the institute played a crucial role in the successful execution of this research.

Following, I would like to thank prof. Andrew Vande Moere, my supervisor at *KU Leuven*, for his guidance and support during the second semester. His expertise and feedback contributed to the development and refinement of this thesis.

Finally, I am deeply grateful to my girlfriend for her unwavering moral support throughout this challenging year, and for her help of proofreading my draft thesis. Her encouragement and belief in my abilities is what has kept me going throughout this study.

Without the collective help and contributions of the individuals and institutions mentioned above, this thesis would not have been possible. I am deeply grateful for their guidance, encouragement, and deep belief in my abilities.



# TABLE OF CONTENTS

ABSTRACT	I
ABSTRACT	III
DANKWOORD	V
ACKNOWLEDGEMENT	VII
1. INTRODUCTION	1
<b>1.1 Problem introduction</b>	<b>1</b>
<b>1.2 Problem statement</b>	<b>1</b>
<b>1.3 Research progress</b>	<b>2</b>
2. LITERATURE STUDY	4
<b>2.1 3D printing</b>	<b>4</b>
2.1.1 Fourth industrial revolution	4
2.1.2 Categories	4
2.1.3 Process	5
2.1.4 Challenges, Advantages and Limitations	7
2.1.5 Conclusion	7
<b>2.2 3D concrete printing</b>	<b>7</b>
2.2.1 Know How and material	8
2.2.2 Different print setups	9
2.2.3 Challenges, Advantages and Limitations	10
2.2.4 Conclusion	11
<b>2.3 Perforated façade</b>	<b>11</b>
2.3.1 Individualized design	12
2.3.2 Increasing use	12
2.3.3 Optimized parameters	12
3. EVALUATION STUDIES	14
<b>3.1 Print set-up</b>	<b>15</b>
3.1.1 Printer range	15
3.1.2 Printer components	15
3.1.3 Programmable logic controller	16

<b>3.2</b>	<b>ABB Rapid Code</b>	<b>18</b>
3.2.1	Tool data	18
3.2.2	Work object coordinate system	18
3.2.3	Target position	19
3.2.4	Move command	19
<b>3.3</b>	<b>Grasshopper</b>	<b>20</b>
3.3.1	Concept	21
<b>4.</b>	<b>PRINT TESTS</b>	<b>22</b>
<b>4.1</b>	<b>Phase 1: How to make perforations with concrete printing techniques?</b>	<b>22</b>
4.1.1	Horizontal printing	23
4.1.2	Vertical printing	26
4.1.3	Printing with incorporation of specialized techniques	29
4.1.4	Conclusion	32
<b>4.2</b>	<b>Phase 2: How to control the <i>Greek Key Shape</i> with different parameters?</b>	<b>33</b>
4.2.1	Orientation	34
4.2.2	Moon shape vs. round shape vs. leaning shape.	37
4.2.3	Width variations	40
4.2.4	Toolpath height and real height	42
4.2.5	Straight layer	44
4.2.6	Greek Key Component	45
<b>4.3</b>	<b>Phase 3: How to control the perforations?</b>	<b>47</b>
4.3.1	Arc panel	47
4.3.2	Toolpath vs. physical results	47
4.3.3	Perforation parameters	48
4.3.4	Side support	51
<b>4.4</b>	<b>Phase 4: How to fabricate a multi-panel design with the <i>Greek Key Pattern</i>?</b>	<b>53</b>
4.4.1	Multi-panel design	53
4.4.2	Closed surface	56
<b>5.</b>	<b>DISCUSSION</b>	<b>58</b>
<b>5.1</b>	<b>Perforations with the <i>Greek key</i></b>	<b>58</b>
<b>5.2</b>	<b>Using the <i>Greek Key</i></b>	<b>60</b>
<b>5.3</b>	<b>Further research and improvements</b>	<b>61</b>
<b>6.</b>	<b>CONCLUSION</b>	<b>63</b>
<b>7.</b>	<b>BIBLIOGRAPHY</b>	<b>64</b>

# 1. INTRODUCTION

## 1.1 Problem introduction

The architecture and construction sector has been known for its conservatism, but with the introduction of digital fabrication methods, the industry is set to undergo a significant transformation (Paoletti, 2017). Among the latest advances in digital fabrication is the novel technology of 3D concrete printing.

One of the major opportunities of 3D concrete printing is that it enables the opportunity of mass customization. By allowing for personalization in the printing process, every object produced can differ from the previous one without adding any complexity to the process (Berman, 2012; Paoletti, 2017). This is because 3D concrete printing creates an object layer by layer, by adding material on the designated place (Wangler et al., 2016). Therefore, this technique shows a great potential in the creation of façades.

A solution and the potential will be explored to create a perforated façade panel with a 3D concrete printer. Facades are one of the most complex parts of a building, offering a personalized touch to every construction (Strauß & Knaack, 2016). The potential of a 3D concrete printer for mass customization aligns perfectly with this objective. Perforated facades allow for the control of solar heat gain, while also providing natural light, making buildings more energy efficient. Moreover, perforated façade panels can serve as a privacy barrier between the interior and exterior spaces (Chi & Doris, 2019).

This research is conducted during the academic year of 2022-2023. The first semester of this year was conducted on an Erasmus+ exchange program at *TU Graz*, Austria. Here, at the *institute of structural design*, a 3D concrete printer was present, which has been used to conduct different test prints. The results from these test prints were carefully measured and photographed. From some test prints, also a 3D scan has been made. The research continued in the second semester at *KU Leuven*, at the *institute for research and design*, including further analysis of the data collected at *TU Graz* and a further literature review on the subject.

## 1.2 Problem statement

This thesis will provide an answer on how to create perforations with a 3D concrete printer and how to control the shape and texture of these perforations. Perforated facades are commonly made of metals, composite resins, ceramics, or bricks (Chi & Doris, 2019). Concrete is also a suitable material for a perforated façade, but it is challenging to create complex shapes due to the need for personalized casting moulds with a high degree of complexity. 3D concrete printing, however, is a construction method that eliminates the need for casting moulds. Complex shapes can be produced without generating any extra complexity to the process (Wangler et al., 2016).

With growing computational power and the use of digital fabrication methods, architects and engineers can now more easily design, calculate, and build perforated facades or façade panels (Rusi, 2019). 3D concrete printing is one of these novel digital fabrication methods.

An increased degree of uncertainty is introduced between the digital input given to the 3D concrete printer, and the physical outcome it produces. Typically, 3D concrete printing involves a horizontal discretization of a geometry and a layered deposition of concrete (Claire Im et al., 2018). In this research, a new method is derived to enable spatial printing with concrete, by introducing vertical movements to the printer. This expands the range of possible outcomes in 3D concrete printing resulting in a new form language. However, introducing vertical movement also increases uncertainty and reduces controllability of the outcome. Therefore, specific solutions are proposed to improve the created method and control how the material will behave under tension to fabricate spatial prints. The increased degree of uncertainty is primarily due to the limited tensile strength of the material before hardening. This uncertain deformation leads to various types of deformation, including bridging, overhanging or uneven deformation, caused by gravity acting on the concrete before it hardens and its own weight. Figure 1.1 illustrates these possible deformations. Bridging occurs when freshly poured concrete spans between two points and starts sagging due to its viscosity and the influence of gravity. Overhanging refers to concrete that is unsupported on one side that falls down under its own weight and gravity. Uneven deformation arises from asymmetric geometries, resulting in unevenly distributed stresses that compress the viscous concrete unevenly (Ko, 2021). This deformation must be considered when fabricating designs using 3D concrete printing technology, especially when creating perforations. To address the challenges of deformation, an accelerator can be added to the concrete mix. Working with such a two-component system facilitates faster hardening of the extruded concrete.

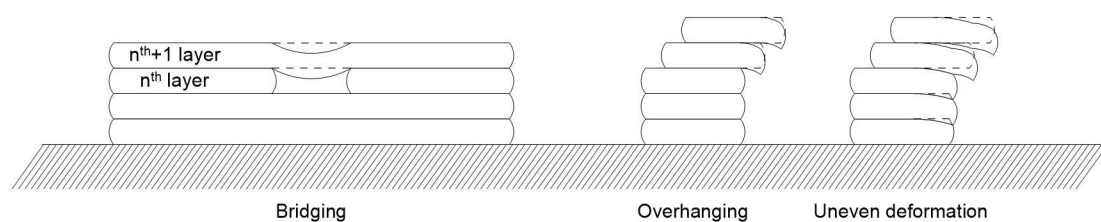


Figure 1.1. Gravity working on the freshly extruded concrete will lead to deformation, under the influence of its own weight and gravity (Ko, 2021).

### 1.3 Research progress

The potential of 3D concrete printing can be broadened with a new form language. This new form is designed to fabricate a perforated façade panel in a faster way compared to traditional construction. With the result of this research, new possibilities in the form language of the concrete printer are possible.

A well-designed perforated wall can create an optimal balance between daylight provision, external views, solar shading, and energy performance of the building (Chi & Doris, 2019). A perforated panel is generally fabricated using digital fabrication methods. The contributions of this research include 1) a validated method for creating and controlling perforations with a 3D concrete printer, with a possibility to generate patterns with the perforations using the parametric design process, and a rough surface texture, 2) a set of parameters for achieving the new form language, and 3) a better understanding of the limitations and challenges of the method. This thesis will contribute to the fast-evolving research subject of 3D concrete printing by proposing an unconventional print method to broaden its possible applications.

This thesis will test the potential of different toolpath techniques in creating perforations and to generate a validated method using computational design software *Rhino Grasshopper*. One of the tested methods will be further explored and tested to achieve an optimized method for creating perforations. By adjusting the given parameters to the algorithm, variations in the perforations or in the panel will be generated.

## 2. LITERATURE STUDY

### 2.1 3D printing

3D printing is a relatively modern technology that has experienced rapid growth over the past few decades. 3D printing, which is often referred to as *additive manufacturing*, is defined by Oxford Languages as the action or process of making a physical object from a three-dimensional digital model, typically by laying down many thin layers of a material in succession (Oxford Languages, n.d.). The first 3D printing machine was created in 1983 by Charles Hull (Hull, 2015). From here on, this technology has rapidly evolved and has known great improvements.

#### 2.1.1 Fourth industrial revolution

According to Xu et al. (2018) and Berman (2012), 3D printing is one of the components of the currently ongoing fourth industrial revolution. An industrial revolution that is characterized as a world where the boundaries between digital domains and offline reality are disappearing. The first industrial revolution started in 1760 with the invention of the steam engine. A great shift happened in the economy from an agrarian and handicraft economy to an economy ruled by industry and machine manufacturing. In 1900, a second industrial revolution happened. This was led by the invention of the internal combustion engine. Oil and electricity made it possible to introduce mass production. The next industrial revolution can be placed from 1960 and is led by the implementation of electronics and information technology. Computers and robotics make it possible to automate production. Now, in the early 21<sup>st</sup> century, the start of a new economical switch is recognized. A fourth industrial revolution that blurs the line between digital, physical, and biological spaces. A revolution that involves computer generated product design and 3D printing. Innovations of this fourth industrial revolution are evolving at an exponential rather than a linear pace (Xu et al., 2018). A shift arises from mass production to mass customization. Mass customization is a new concept that puts together the two contradictory notions “mass” and “customization” (Paoletti, 2017). This explains a fast and rapid production of personalized and customized products, at low costs. 3D printing enables users to easily print personalized parts without adding any complexity to the production process (Berman, 2012; Wangler et al., 2016).

#### 2.1.2 Categories

*The American Society for Testing and Materials* (ASTM) states that 3D printing can be classified into seven different categories, according to the used material and the print method (Ko, 2021; Zhang & Liou, 2021). Table 2.1 gives an overview of these classes, together with the generally used power source and most printed materials for these classes. Every class uses a different print method and offers specific advantages or disadvantages compared with different print methods. A further explanation of all these different classes would guide us to far from the topic of this thesis.

Table 2.1. Classification of 3D printing according to the American Society for Testing and Materials (Zhang & Liou, 2021).

	CATEGORIES	POWER SOURCE	MATERIALS
<b>I</b>	Vat Photopolymerization	Ultraviolet light	Photosensitive resin Ceramics
<b>II</b>	Material Jetting	Thermal energy	Photopolymer resins Metals Ceramics
<b>III</b>	Material Extrusion	Thermal energy	Thermoplastics
<b>IV</b>	Binder jetting	Binder/Thermal energy	Polymer Ceramic Metal powder
<b>V</b>	Powder bed fusion	Laser Electron beam	Polymer Ceramic Metal powder
<b>VI</b>	Sheet lamination	Laser	Plastic Metal Ceramic foil
<b>VII</b>	Directed energy deposition	Laser	Metal Ceramic powder

Concrete printing, as will be further described in section 2.2 (“3D concrete printing”), is a variation on material extrusion. The power source for this will not be on thermal energy but on natural hardening. The printing method will be similar to *Material extrusion* as the material will be extruded through a nozzle (Ko, 2021).

### 2.1.3 Process

3D printing, or additive manufacturing, is a construction method in which material is added to create an object generated in a digital model. This is done by successively adding material in a layer-by-layer fashion (Zhang & Liou, 2021). Additive manufacturing is the opposite of subtractive Manufacturing, which start from a solid block, bar or rod that is shaped by removing material through cutting, boring, drilling and grinding (Paoletti, 2017).

The general steps in the process of 3D printing are the same for every different printing method. Figure 2.1 gives a graphical representation of these different steps. These can be described as followed (Zhang & Liou, 2021):

#### 1) Creating CAD file

The most generally used approach for creating a digital model is with CAD software. CAD software allows the user to generate 3D models of every shape possible.

#### 2) Exporting to STL file

When the 3D model is fully finished in the CAD software, it needs to be exported as an STL file (Standard tessellation language). This is a file type that only contains the surface geometry of a 3D object. It is represented by a number of triangular facets with normals and vertices.

#### 3) Slicing of the STL file

The STL file can be uploaded in a slicing software (e.g., Ultimaker Cura, Simplify3D, PrusaSlicer...). In this software, the geometry is sliced into a number of horizontal cross sections (layers).

#### 4) Toolpath and G-code generation

The formed cross sections (layers) are formed to a toolpath. This is the path that the printer will follow while printing the object. This toolpath is translated into movements for the robot, described as G-code. This algorithm considers many factors such as the selection of infill patterns, heat, input profile etc.

#### 5) Set-up of the printer and actual build

The 3D printer is set-up. The right parameters and settings are inserted for the print (e.g., material type, power, layer thickness, traveling speed, building plate temperature, support). Once this is completed, the actual layer-by layer build of the object can start. After one layer is built, the extruder moves up or the print bed moves down by a layer thickness so that another layer can be deposited. The printing process is largely automated. No constant supervising is needed.

#### 6) The printed object is removed from the 3D printer.

The printed object can be removed from the 3D printer. According to the chosen print method, this can be taking it out of a powder bed, taking it out of a resin bed or simply removing it from the print bed.

#### 7) Post processing

Depending on the used printing method, the used material and the future application of the printed object, post processing might be needed. This can be the removal of support, sanding, polishing, CNC milling, chemical dipping, filling... This is not needed for every print.

#### 8) Application and use of printed objects

The printed objects are completed and can be used for the planned application.

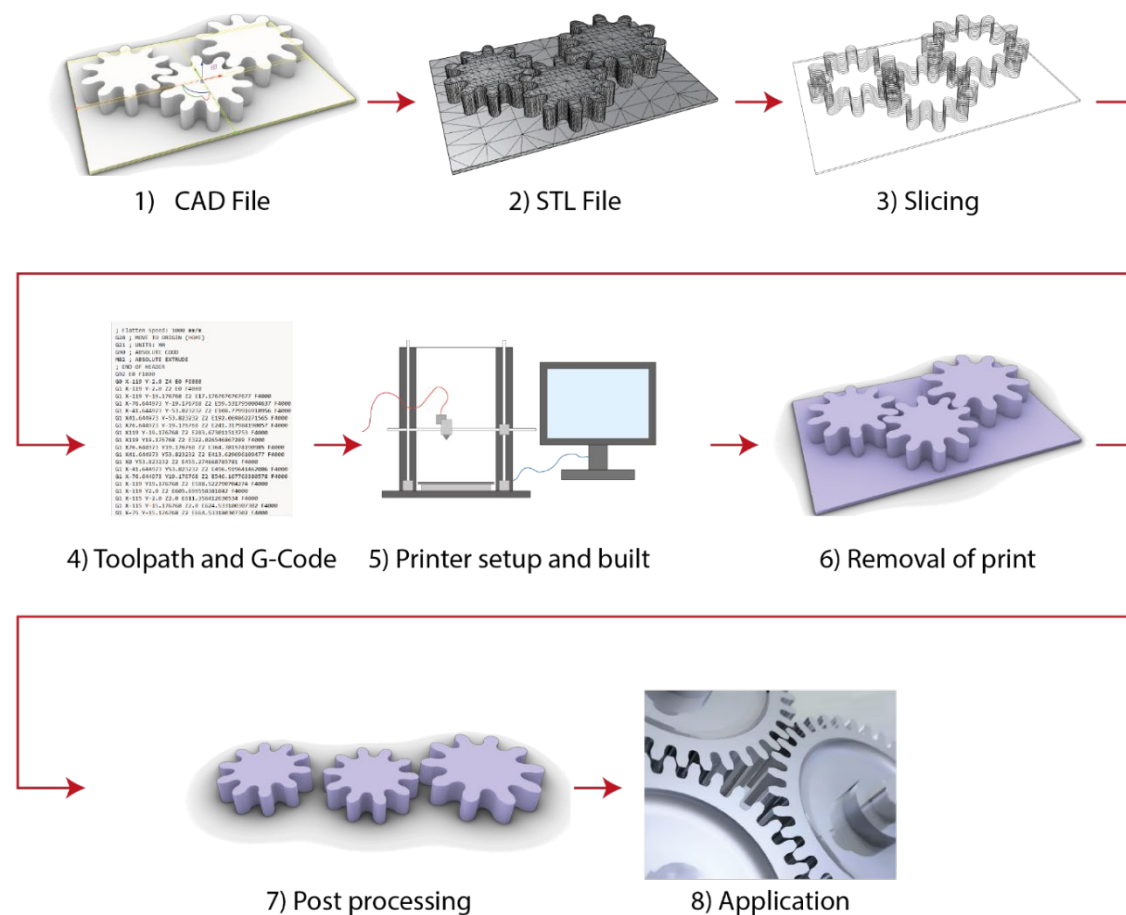


Figure 2.1. 3D printing process is based on eight consecutive steps, in order to obtain a 3D printed object from a digital model.

### *2.1.4 Challenges, Advantages and Limitations*

There exist three primary manufacturing processes: Additive manufacturing (e.g., 3D printing), Subtractive manufacturing (e.g., turning, drilling, milling etc.) and Near net shape processes (e.g., stamping, casting, injection, blow moulding, thermoforming etc.). Each manufacturing process shows its own characteristics and applications (Kosky et al., 2021). The main advantage of 3D printing is the ability and flexibility in product design, where there are almost no limits. The layer-by-layer construction permits the creation of complex shapes that may not be achievable with e.g., CNC (Sarakinoti et al., 2018; Zhang & Liou, 2021). Since the printed model can be easily modified in any CAD software, it is ideal for mass customization. This makes it perfect for small quantities of products that can all be distinct from each other. Variations in the objects being printed do not slow down the print process, as they are constructed from layer-by-layer contours (Berman, 2012). The digital input or CAD file is easily transferable online and shared between different parties. If these parties have their own 3D printer, they can all print their own version (Berman, 2012). Several open-source platforms (e.g., Thingiverse, Pinshape, Printables etc.) already exist, where users can share their own designs. Once the printer is started, it is an automated manufacturing process, requiring minimal manual intervention. Only after the printing process is completed, it must be removed and treated with the post processing process (Zhang & Liou, 2021). This significantly reduces labour costs compared to other manufacturing methods (Berman, 2012). Furthermore, since the material is only deposited where it is needed, there is almost no material waste (Berman, 2012).

However, 3D printing has some limitations and disadvantages. It is not suitable for mass production, as it can only produce one product at a time (Berman, 2012). The manufacturing of a product takes longer than traditional manufacturing processes, however, the overall path from digital model to physical product is shorter (Ghasemieshkaftaki et al., 2021; Zhang & Liou, 2021). The world of 3D printing is continually evolving, with a lot of innovation taking place. Although it is currently possible to print with various materials, there are still limitations since not every material is suitable (Berman, 2012). Structurally, the printed objects will have an anisotropic material structure due to the layer-by-layer build. The maximum strength will also be lower than that of traditional manufacturing methods (Zhang & Liou, 2021) In order to achieve high precision as with other production methods, expensive 3D printers are required (Zhang & Liou, 2021).

### *2.1.5 Conclusion*

Before developing and producing a product, careful consideration is necessary regarding the advantages and disadvantages of this production method. It is essential to note that 3D printing is a relatively new technology that is currently under extensive development. As such, new improvements are being made to this technology continually (Xu et al., 2018).

## **2.2 3D concrete printing**

Concrete is the second most widely used material in the world after water, with an estimated annual usage of approximately two billion tons. Concrete is a mixture of fine and coarse aggregates, cement, and water at a certain ratio. Its popularity stems from its ability to transition naturally from a fluid state to a solid state, allowing it to flow and fill a mould and sustain a load upon hardening (Ko, 2021; Wangler et al., 2016).

Architecture and construction are one of the most withholding sectors to changes. Therefore, advanced manufacturing technologies and innovative production methods are often neglected or postponed within this field, due to the prevalence of traditional construction methods and consolidated processes that prioritize economic considerations over the effective need of innovation and improvement. Nevertheless, digital technologies are gradually finding their place in the field of construction and architecture (Paoletti, 2017). 3D concrete printing has emerged as a promising innovation in this regard. 3D printing has already proven successful in printing polymeric materials extruded in a liquid state and subsequently hardened, as explained in the previous chapter “3D printing” (Wangler et al., 2016).

The application of 3D concrete printing has the potential to bring new aesthetics and sustainable qualities in architecture and construction (Bekkering et al., 2020). Older buildings come from a time when craftsmanship prevailed and facades were ornamented with sculpture and carvings. These qualities have become increasingly rare and are only found on special building, due to rising labour costs and the emphasis on mass production in the wake of the industrial revolution (Strauß & Knaack, 2016). However, 3D concrete printing has the possibility to once again fabricate complex shapes and ornamentation, as the printing process makes complicated shapes and labour-intensive machining processes possible again (Bekkering et al., 2020).

### 2.2.1 Know How and material

To successfully utilize 3D concrete printing in design, it is essential to have a thorough understanding of the capabilities and limitations of the printer and the material. This includes knowledge of the angles of inclination that can be printed, the challenges of the continuous printed line and the limitations imposed by gravity and the curing process of the material. In addition, proficiency in software programs such as *Rhino Grasshopper* (Rhino Grasshopper, 2022) for parametric design and as well as software programs for printer operation is crucial. When creating a design, the limitation of the toolpath needs to be taken in consideration. The toolpath always needs to follow one continuous line, overlapping of this line will create imperfections and the toolpath between two points must follow the restrictions of the printer. The final print will also not show straight corners. These will always be rounded in the print (Bekkering et al., 2020).

The biggest challenge for 3D concrete printing is the material itself. It must be soft enough to intermix with the previously deposited layer, yet hard enough to support its own weight and the weight of the material from the layers deposited on top. The initial Yield stress  $\tau_{0,0}$  of any layer must be strong enough to support itself. This can be defined as:

$$\tau_{0,0} = \frac{\rho g h}{\sqrt{3}} \quad eq.2.1$$

Where  $\tau_{0,0}$  is the initial yield stress,  $\rho$  the density,  $g$  the gravity constant and  $h$  the layer height.

The final Yield stress must be strong enough to carry the entire height  $H_m$ . This can be shown in a formula as follows:

$$\tau_{0,f} = \frac{\rho g H_m}{\sqrt{3}} \quad eq. 2.2$$

Where  $\tau_{0,f}$  is the final yield stress,  $\rho$  the density,  $g$  the gravity constant and  $H_m$  the entire height (Malaeb et al., 2019; Wangler et al., 2016).

Cold joints can be described as a weak connection between two consecutive layers of concrete. This can occur when two successively casted layers of concrete fail to intermix sufficiently. This can happen when a critical resting time is exceeded, and the previous layer is no longer viscous enough to intermix with the new layer. This defines a maximum time for a layer to be produced (Wangler et al., 2016).

### 2.2.2 Different print setups

There are various print setups that can be used for 3D concrete printing. An example of some systems is given in Figure 2.2. This is for example a) a cartesian robot (syn. gantry robot), b) a cylindrical robot, c) a spherical robot (syn. polar robot), d) a scara robot, e) a delta robot, or f) a robot with rotary joints (syn. robotic arm) (Ko, 2021).

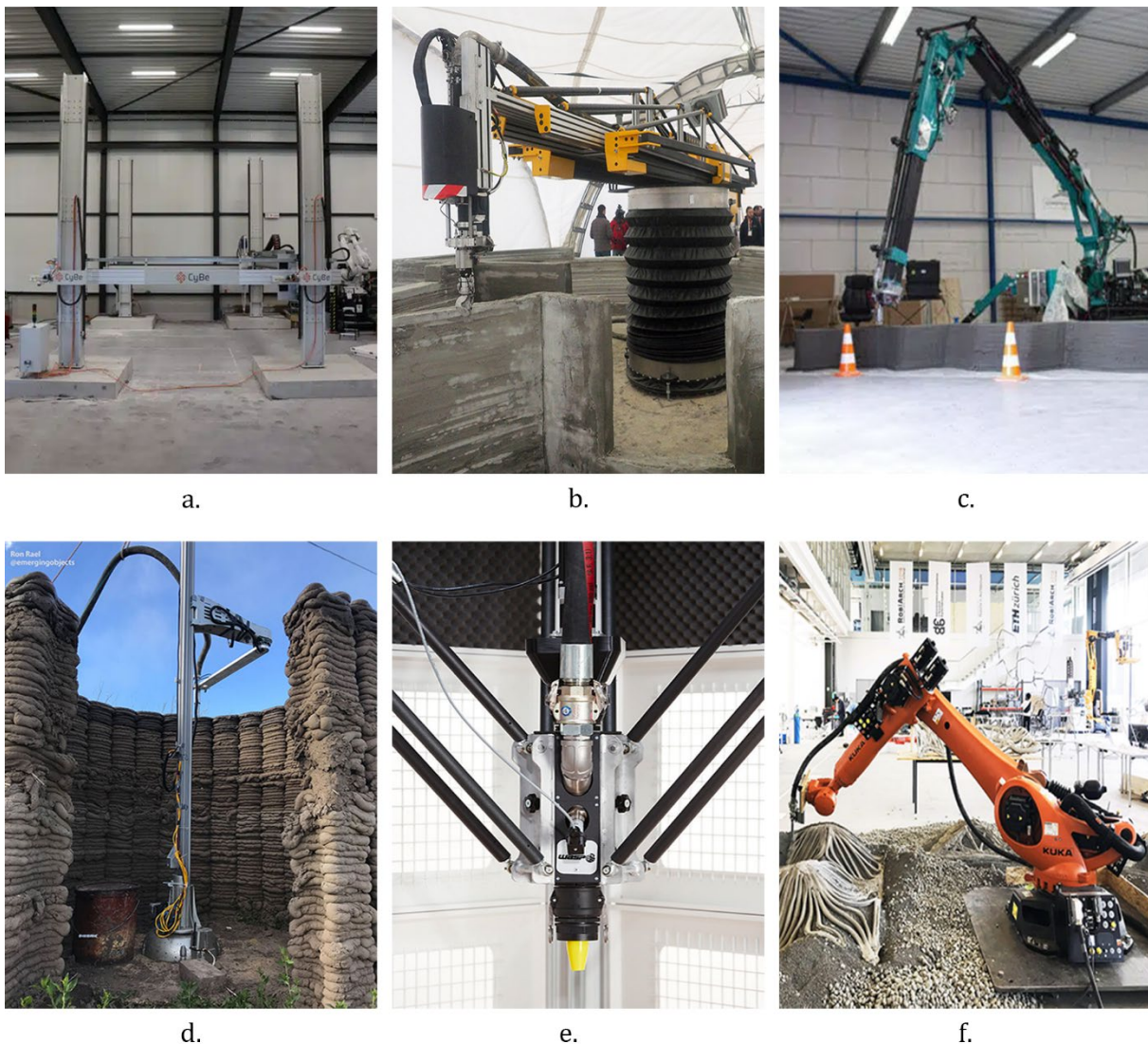


Figure 2.2. Different print setups: a) Cartesian system, b) cylindrical system, c) spherical system. d) scara system, e) delta system, f) rotary joints system. Each allowing for different movements and qualities (3D Potter, n.d.; Chen, 2019; Constructions-3D, n.d.; Cybe Construction, 2018; Ko, 2021; Wasp, n.d.).

Cybe Construction and Zant et al. (2018;2023) give some extra variations on this last setup with rotary joints. This includes f.1) a fixed system, f.2) a mobile system with rubber tracks, f.3) an extra linear track system or f.4) a combination of rotary joints, mounted on a gantry system. Figure 2.3 gives an example of each of these different print setups. The print systems can vary in speed, degree of freedom, different print range, on- or off-site printing and more (Zant et al., 2023).

Additionally, there are differences in print setup between single-component systems and two-component systems resulting in different material behavior upon extrusion. Single-component systems will use a ready-mix concrete with no additional additives resulting in highly viscous concrete, while two-component systems will add an additive to the concrete mix, typically an accelerator that speeds up the hardening process so it can carry the needed initial yield stresses. This is often added inside the nozzle (Wangler et al., 2016).

3D concrete printing is possible for both on-site as off-site printing but is in most cases used for prefabrication. The elements are printed off site and are, after the curing process, moved to the desired location. This technology works with the layer-by-layer method, similar to 3D printing. The layer heights of 3D concrete printing generally measure a few millimetres or even centimetres, which makes the scale larger compared to 3D printing where layers are of the scale of a couple of millimetres or even micrometres (Wangler et al., 2016).

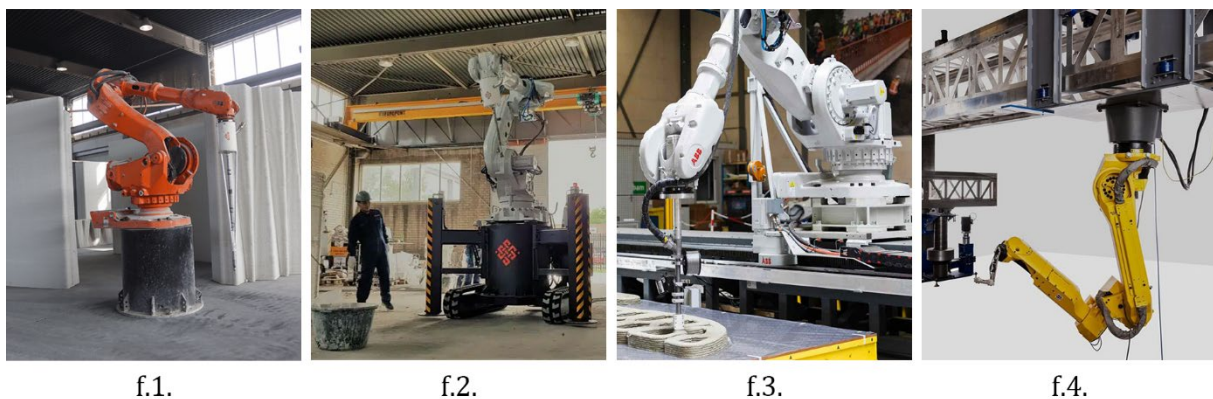


Figure 2.3. Different print setups variations on the rotary joint system: f.1) fixed system, f.2) mobile system, f.3) track system, f.4) gantry system with rotary joints. (Cybe Construction, 2018; Stevenson, 2021)

### 2.2.3 Challenges, Advantages and Limitations

Like traditional 3D printing techniques, 3D concrete printing offers several advantages and disadvantages, as well as some challenges. Some of these are similar to those of traditional 3D printing.

For example, one of the key benefits of 3D concrete printing is the possibility to fabricate freeform architecture and organic ornaments. The digital process and layer-by-layer built allow for the creation of unique and intricate shapes, without adding any complexity to the printing process. By varying the print path during the printing process. Different surface patterns can be implemented on the printed object. Once the printer is running, the process is mostly automated. Requiring minimal interference until the print is finished. This reduces the risk of human error and allows for the creation of complex structures with high precision and accuracy. 3D concrete printing will also help reducing construction time. This will be because a robot can work non-stop while workers only work shifts. This will lead to a reduction in manual labour, making the construction more cost effective, since labour costs take up about 25%-35% percent of the project costs. This will also reduce the risk of accidents and injuries because of the automated process. Furthermore, there is no longer need for castings in this process. So, no material on castings will be lost. Additionally, the technology allows for efficient structural design, resulting in stronger, lighter, and more durable structures. Another advantage of 3D concrete printing is the reduction in waste material. This technology only extrudes precis amounts of material where it is needed, leading to minimal waste. These advantages make that 3D concrete printing is believed to lead to more sustainable construction (Bekkering et al., 2020; Ko, 2021; Malaeb et al., 2019; Wangler et al., 2016).

However, like any new technology, 3D concrete printing has its limitations and challenges. Cracking during the drying process when building with concrete is a potential problem. This can occur due to differences in temperature, humidity levels, as well as poor concrete mix design. This problem also shows when using concrete for the 3D concrete printer. The layer-by-layer built will result in a layer-built surface finish if no postprocessing is applied. Another disadvantage would be the lack of reinforcement in 3D concrete printing. In current research, tests have proven positive with a special nozzle that can insert reinforcement during a print. This is however still limited to small reinforcement cables, only in the same direction as the toolpath. Small fibres in the concrete mix provide a first solution against cracking. Just as other 3D printing processes, the element size that can be printed is limited by the size of the printer. This makes that a 3D printer often needs to be relatively big in order to print most objects. The mechanical strength of the concrete is weak before setting. This could impact the final product upon drying. Weak connection between layers, known as cold joints, result in an overall weak object. Finally, there is a need for specific Know How, which may limit the widespread adoption of 3D concrete printing in the construction industry (Ko, 2021; Schmidt & Slowik, 2009; Wangler et al., 2016). Table 2.2. gives an overview of the above mentioned advantages and limitations.

Table 2.2. Advantages and limitation of 3D concrete printing.

ADVANTAGES	LIMITATIONS
<ul style="list-style-type: none"> <li>• Freeform architecture</li> <li>• Different surface patterns</li> <li>• Automated process</li> <li>• Small risk for human error</li> <li>• High precision and accuracy</li> <li>• Reduces construction time</li> <li>• More cost-effective construction</li> <li>• Provides more labour safety</li> <li>• No formworks needed</li> <li>• Efficient structural design</li> <li>• Less construction waste and carbon emission</li> </ul>	<ul style="list-style-type: none"> <li>• Cracking in the drying process</li> <li>• Layer-built surface finish</li> <li>• Reinforcement is difficult/limited</li> <li>• Print size limited by printer</li> <li>• Limited mechanical strength before setting</li> <li>• Cold joints</li> <li>• Specific Know How</li> </ul>

#### 2.2.4 Conclusion

3D concrete printing is a promising technology that offers new benefits to architecture and construction compared to traditional construction methods. Although there are some limitations and challenges, further research can keep improving this technology and expand the range of applications of 3D concrete printing (Bekkering et al., 2020).

### 2.3 Perforated façade

The façade is an integral and multifaceted component of a building. It separates the interior from the exterior environment, so that the internal conditions can be maintained, and the energy consumption can be maintained to a minimum. A well-designed façade will provide an acoustic barrier, maintain the temperature differential between interior and exterior, resist wind and rain and will function as a hygrothermal barrier (Mendonça & Macieira, 2019; Strauß & Knaack, 2016). The quality of the façade can significantly impact a building's energy consumption and indoor environmental quality (Ghasemishkaftaki et al., 2021). Additionally, the façade gives a face to the building. It gives the representation of the design intent between the customer, the architect, and

the user. The form language of a façade is as important as the quantitative performances because it can influence the first impression of the building (Kim et al., 2017; Strauß & Knaack, 2016).

### *2.3.1 Individualized design*

This diversity of functions of the façade makes this one of the more challenging parts of a building, whereas architects and engineers need to find a balance between architectural design and functionality (Ghasemieshkaftaki et al., 2021; Mendonça & Macieira, 2019). Each façade has its own individual character and is a “one of a kind”. The use of computational tools enables engineers to experiment with new configurations and optimize the distinct functions of a façade (Rusi, 2019). As seen in the previous chapters: 3D printing is an ideal solution for this type of individual customization. 3D printing will most likely start playing a more important role in façade construction and can help reduce the required resources, labour costs and construction time, while facilitating more complex forms (Ghasemieshkaftaki et al., 2021; Strauß & Knaack, 2016).

The choice of materials and design configuration of a façade is critical for achieving energy efficiency and natural light control. Static facades with solid walls and a high mass will help reduce heat transmission loss but will block all-natural light. Artificial lighting will be required in this case, resulting in more energy consumption. Conversely, fully glazed buildings cause significant heat transmission loss during the winter and excessive solar gain in the summer (Ghasemieshkaftaki et al., 2021). Chi and Doris (2019) add to this that fully glazed buildings are, in general, more appealing but ignore their climatic conditions. A well-measured balance between glazed and solid walls must be found. Perforated walls offer a good solution for this. A well-designed perforated wall can create an optimal balance between daylight provision, external views, solar shading, and energy performance of the building. A perforated wall is mostly constructed of two layers, a structural layer, and a perforated layer, which often are perforated panels. perforated panels are mostly placed in front of a glazed wall or window to perceive a contemporary look and to meet the expectations of visual and lighting passage (Chi & Doris, 2019).

### *2.3.2 Increasing use*

The last years, use of perforated patterns in facades is increasing (Kim et al., 2017). Rusi (2019) explains this phenomenon by the increasing collaboration among professionals in a co-design and says it is rising in conjunction with the rise of digital technology. New design tools enable architects to easier explore complex geometries for façades and experiment with different perforations. A perforated panel is an opaque lattice with perforations that can vary in shape, size, number, and distribution. the most common materials, used for a perforated façade are metal, composite resin, ceramic or brick. It is however not limited to these materials (Chi & Doris, 2019).

### *2.3.3 Optimized parameters*

A perforated façade is well suited for allowing solar control, while at the same time providing adequate daylight indoors. Daylight stimulates the visual and circadian systems and produces a positive psychological effect on occupants. The provision of daylight and sunlight also reduces artificial lighting and provides sufficient heat to decrease the active thermal conditioning system. Most architects follow an aesthetic and morphological thinking while designing these panels and do not consider the ideal distribution of the perforations (Chi & Doris, 2019). However, it is important to know the screen parameters and their influence, such as panel thickness, perforation percentage, separation distance between the glazed wall behind it and others. The most important key is the orientation of the perforated panels. This directly impacts the amount of daylight that can be transmitted through all the perforations. the next thing to consider while designing a

perforated surface would be the organization and distribution of the holes. They filter out incident direct sunlight. The shape of the holes does not really influence the result or energy performance of a building. Next part to consider is the thickness of a panel and the spacing between the panels and the glazed wall. Chi & Doris (2019) have given a summary of the optimum values for the perforated percentage, the thickness of the panel and the distance to the glazed wall in their research. This is shown in Table 2.3 and is divided in east, south and west.

Table 2.3. Optimum values for a perforated façade (Chi & Doris, 2019).

	EAST	SOUTH	WEST
PERFORATION PERCENTAGE	40% - 50%	20% - 50%	40% - 50%
THICKNESS	7 cm	3cm - 7cm	3cm - 7cm
DISTANCE	120cm	90cm - 120cm	60cm-120cm

Various methods exist for calculating the amount of light transmitted through a perforated panel. One approach involves determining the quantity of direct sunlight that passes through the panel. This can be expressed as:

$$\text{Transmitted light} = \text{Incident light} * \frac{\text{Perforated area}}{\text{Panel area}} \quad \text{eq. 2.3}$$

It is worth nothing that this technique is a simplified method, as it does not account for any degree of reflection. As such, the results from this equation will be an underestimation of the actual values (Kim et al., 2017). This formula will, in the continuous of this research, be used to give an approximation of the light transmitted through perforated façade panels.

### 3. EVALUATION STUDIES

The first part of this research consisted of a comprehensive literature review, with the focus on 3D printing technology and a specific emphasis on 3D concrete printing (3DCP). Reference projects that have been created using concrete printers are analyzed in detail to gain insights into the potential of 3DCP. From this a first conception on the possibilities with 3DCP is formed. This literature study also included an examination of the process of 3DCP. How this starts from a digital geometry to a printable object for the robot.

Following the literature review, a self-study was conducted using *Rhino Grasshopper* software. Tutorial videos were used to gain knowledge with the software. To address specific problems I encountered, the McNeel forum (Robert McNeel & Associates, n.d.) was used. This site included forum posts on similar problems as the problems I encountered while working and designing in *Rhino Grasshopper*.

The knowledge acquired from the literature review and self-study in *Rhino grasshopper* was then applied to practical tests conducted with the 3D concrete printer at *TU Graz*. The practical tests consisted of four phases.

#### **Phase 1: How to make perforations with concrete printing techniques?**

Seven toolpath techniques are evaluated, introducing a variety of potential methods to fabricate perforations. The used parameters to define the algorithm are carefully noted. In some cases, the parameters are changed, and a second test print was performed. From these toolpath techniques, one is further developed in the subsequent phases of this research. This toolpath technique will be referred to as the *Greek Key* in the continuous of this research.

#### **Phase 2: How to control the *Greek Key* with different parameters?**

The *Greek Key* is further analyzed in this phase by printing single lines with this shape. These lines will depict varying orientations and parameters. This way, different outcomes of the *Greek Key Shape* are derived. Results from this phase will give a broader knowledge on how to control a singular *Greek Key Shape* and how this can be manipulated to specific designs.

#### **Phase 3: How to control the perforations?**

In this phase, the focus will be on creating panels with the *Greek Key Geometry*. Multiple lines, consisting of the *Greek Key* are printed on top of each other. The effects of varying the parameters that control the perforations are observed. Knowledge on the fabricated perforations is obtained, as well as some design criteria for using the *Greek Key Shape* in a panel design.

#### **Phase 4: How to fabricate a multi-panel design with the *Greek Key Pattern*?**

With the knowledge from the previous phases, a first attempt is made to a fictional design made with multiple 3D printed panels using the perforations as described in this research. Improvements for a future test are proposed to avoid failures of design with the *Greek Key Pattern*.

### 3.1 Print set-up

For this research, practical tests are conducted at the processing robot facility at *TU Graz*. This facility is part of the faculty of architecture and is run by the *Institute of Structural Design* (ITE).

The facility houses an industrial robotic arm from ABB, specifically the IRB 6660 type. This industrial robot is well suited for high performance applications. A stiff design offers a high accuracy up to  $\pm 0.2\text{mm}$ . This makes the robot ideal for applications as machining, milling, grinding, cutting, sawing or other applications (ABB, 2020). In this facility, the robot is mostly used for additive manufacturing, also called 3D printing, with concrete. The stiff design of this robot makes that the maximum allowed acceleration on this robot is lower than on traditional robots. This can cause some imperfections in the additive manufacturing process (ABB, 2020). Examples of these imperfections will follow in 4.1.1 (“Horizontal printing”). This robotic arm is a six-axis robot, and has, as the name suggests, six rotating axes. These axes are marked in Figure 3.1. This makes that the robot can move flexible and can work in all angles (Bernier, 2021).

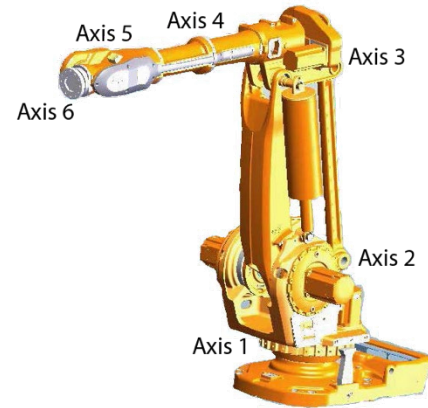


Figure 3.1. The processing robot facility at *TU Graz* houses an ABB IRB 6660 6-axis robot for their 3D concrete printer (ABB, 2020).

#### 3.1.1 Printer range

The industrial robot at the processing robot facility in Graz is provided with a seventh high precision linear axis, designed by Nomotec (see Figure 3.2). This extra axis has a length of 7400mm, making it possible for the robot to process along a length of 6000mm, giving it a total processing area of 6000 x 1200 x 1200 mm. At the ABB control unit, this seventh axis can be enabled or disabled. When the linear axis is enabled, the industrial robot has a larger reach, but the maximum processing speed will be more limited (Institute of Structural Design, n.d.). With no 7<sup>th</sup> axis, the maximum speed, according to ABB, can go up to 6000mm/s. With this seventh axis enabled, the maximum speed gets limited to 250mm/s. It is to be noted however that the maximum applied speed in the following research was at all times limited under 600mm/s.

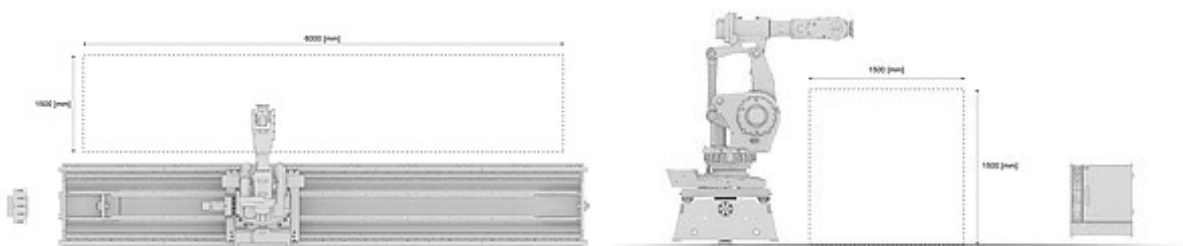


Figure 3.2. A seventh axis of 7400 mm on the ABB six-axis robot enlarges its process area to 6000 x 1200 x 1200 mm (Institute of Structural Design, n.d.).

#### 3.1.2 Printer components

A 3D concrete printing system from Baunit is used. This system is a two-component system, in which mortar and an accelerator are mixed in the nozzle. This extrudes a rapidly stiffening concrete mix. The full printing system consists of multiple machine components. A diagram (see Figure 3.4), provided by the ITE shows all the components in this installation. This includes a print

nozzle, a programmable logic controller (PLC), a hydraulic unit, accelerator pump, mortar mixing pump and a kinematics control unit (KCU), which some are shown in Figure 3.3.

Baumit printing mortar (PRINTCRETE 230) is poured into the mortar pump. This mortar pump mixes the mortar with the right amount of water. This mortar is then sent, with pressure, through a tube to the Baumit print nozzle. In the nozzle, the mortar gets mixed with a chemical admixture: accelerator, which is pumped through a dosing pump to the print nozzle. This accelerator makes that the concrete sets faster (Strieder, 2005), making it possible to print layers on top of each other, without the concrete failing. In this case, a nozzle was used with a diameter of 14mm. The robotic arm is controlled from a kinematics control and can either be set on automatic or manual mode. In manual mode, the maximum speed of the industrial robot will be limited. The print nozzle is mounted onto the robotic arm and from a programmable logic controller (PLC), everything is controlled. This PLC controls the amount of material, amount of accelerator, pressure, maximum speed etc. and sends all this information to the right component (ABB, 2020; Institute of Structural Design, n.d.).



Figure 3.3. Different components of the 3D concrete printer setup at TU Graz. From left to right, top to bottom: BauMinator print nozzle, PLC, KCU, Mortar pump and Kinematics controller.

### 3.1.3 Programmable logic controller

The Programmable Logic Controller (PLC) serves as the central station for the 3D concrete printer, allowing for the precise adjustment of various parameters, under which the robot speed, acceleration input, concrete extrusion speed and others. The robot speed is measured in mm/s.

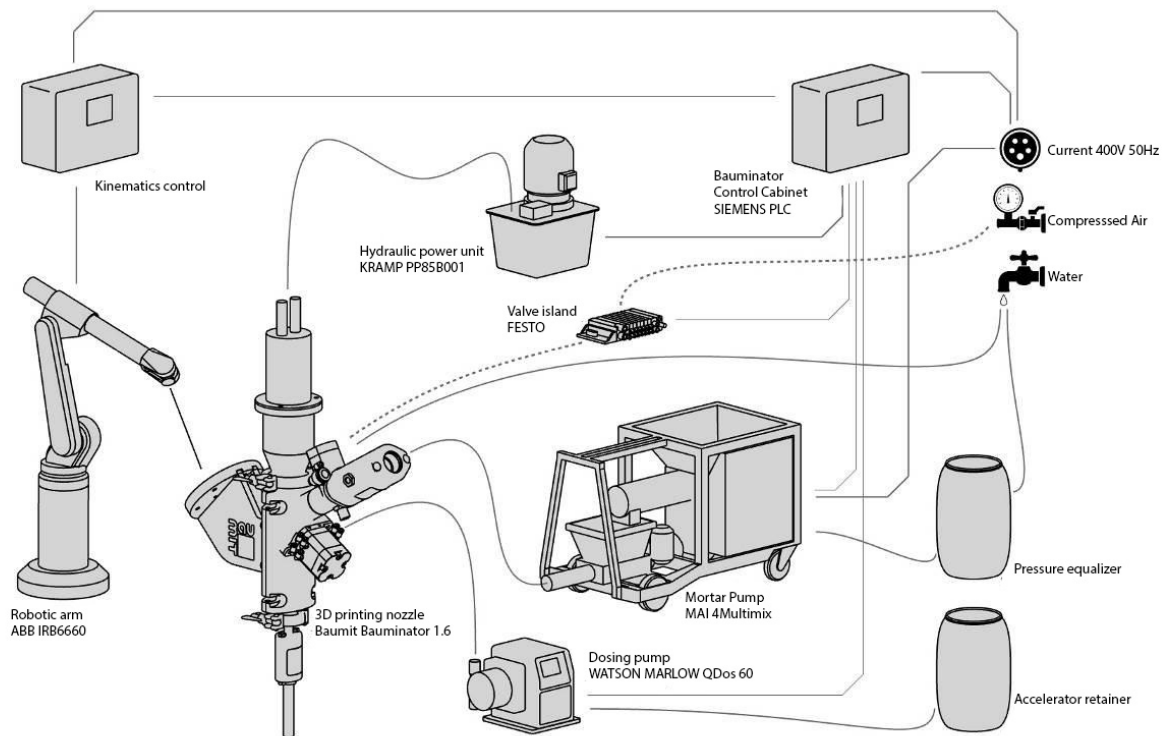


Figure 3.4. Printer setup at TU Graz, explaining the interrelation between the different components (Institute of Structural Design, n.d.).

Decreasing the robot speed, the printer's movements become slower, resulting in a higher amount of material extrusion along the print path. Conversely, increasing the robot speed leads to faster movements and less thin printed lines. However, it is to be noted that the acceleration speed of the printer remains constant. When dealing with many short print lines, such as the *Greek Key*, the printer may not have enough time to fully accelerate, resulting in a constant limited speed of the robot and an inability to achieve the maximum defined speed.

The accelerator input determines how quickly the concrete mix hardens upon extrusion. A higher accelerator value causes the concrete to cure faster, enhancing its resistance to shear forces. However, this may reduce its ability to intermix with other layer of concrete. The accelerator is expressed in "% of the concrete mix" and generally ranges between 4% - 6%.

The amount of extruded material is specified in hertz [Hz]. Within the mortar pump, a worm screw, as shown in Figure 3.5, rotates at a given frequency, effectively pumping the material towards the printer. A linear relation exists between the amount of extruded material and the rotation of the worm screw. To convert the rotation speed into litres per second, the following formula is applied:



Figure 3.5. A worm screw in the mortar pump rotates and pushes the concrete towards the print nozzle.

$$\text{extruded material} = \frac{\text{rotation speed}}{1000} + 0,005 \quad \text{eq. 3.1}$$

Throughout this research, commonly used rotation speeds are 27Hz, 30Hz and 35Hz, corresponding to material extrusion rates of 0,032l/s, 0,035l/s and 0,04l/s, respectively.

## 3.2 ABB Rapid Code

The industrial robot is controlled with ABB rapid code. A brief explanation will follow on some basic concepts to understand how this works. This code will define every movement from the robot. But before the movements can be coded, other concepts need to be defined in the beginning of the code. This is defined as *Persistent*. A persistent code line is preceded by `PERS`. This includes for example information of the tool mounted on the robot and the coordinate system of the work object.

### 3.2.1 Tool data

In this case, a print nozzle is mounted on the end of the robot. The tool coordinate system and characteristics of this nozzle can be defined relatively to the robot. This can be defined as `tooldata`.

```
PERS tooldata Toolname:=[True/False, [[X,Y,Z], [q1,q2,q3,q4], [kg, [Xe,Ye,Ze], [1,0,0,0], i1,i2,i3];
```

Toolname
Robot Hold
TCP
Orientation
Physical Info

With:

Table 3.1. Components for Tool Data (ABB, 2004; Raspall, 2013).

Name	Definition
Toolname	Specific name given to this tool
Robot Hold	Defines whether or not the robot is holding the tool. [Boolean]
Tool Coordinate System	
- Tool Coordinate Point (TCP)	The position of the centre point of the tool, relatively to the end of the robot arm. [mm]
- Orientation	The orientation of the coordinate system of the tool, relatively to the wrist coordinate system of the robot. [°]
Physical info	Physical weight of the tool, Centre of mass of the tool, Moments of inertia.

### 3.2.2 Work object coordinate system

Another aspect to define in the rapid code is the coordinate system of the area the robot will work in. this coordinate system will be moved and rotated, relatively to the base of the robot. This can be recognized in the rapid code as:

```
PERS wobjdata AreaName := [True/False, [[X1,Y1,Z1], [q11,q12,q13,q14], [X2,Y2,Z2], [q21,q22,q23,q24]];
```

Coordinate System Name
Robot Hold
Position
Rotation
Position
Rotation

With:

Table 3.2. Components for work object coordinate system (ABB, 2004; Raspall, 2013).

Name	Definition
Coordinate system name	Name for this specific coordinate system
Robot Hold	Defines whether or not the work object is held by the robot. [Boolean]
User frame Coordinate system	
- Position	Position of the origin of the coordinate system [mm]
- Rotation	Rotation of the coordinate system [°]
Object frame Coordinate system	
- Position	Position of the origin of the coordinate system [mm]
- Rotation	Rotation of the coordinate system [°]

### 3.2.3 Target position

Next, there will be a focus on target positions of the robot and movements. A target position defines a position in which the robot will be after this code line. This is defined as `robtarg` and will look like:

```
CONST robtarg TargetName := [[X1Y1Z1],[q1,q12,q13,q14],[cf1,cf4,cf6,cfx],[9E9,9E9,9E9,9E9,9E9,9E9]];
      |           |           |           |           |
      | Target Name | Target | Target | Target | External Axis
      | Position   | Position Orientation Configuration
```

With:

Table 3.3. Components for target position (ABB, 2004; Raspall, 2013).

Name	Definition
Target name	Name for this specific target point.
Target position	The position of the tool centre point [mm]
Target orientation	The orientation of the tool [quaternion]
Target configuration	The axis configuration of the robot [°]
External axis	The position of the external axes. [° or mm] – 9E9: defined for axes which are not connected.

### 3.2.4 Move command

To move the robot, there are multiple variations. The most used commands are `MoveL`, `MoveC` or `MoveJ`. Each command defines a different type of movement.

Table 3.4. Different move commands (ABB, 2004; Raspall, 2013).

<code>MoveL</code>	Used to move the tool centre point (TCP) linearly to a given destination
<code>MoveC</code>	Used to move the tool centre point (TCP) in a circular motion to a given destination
<code>MoveJ</code>	Used to move the tool centre point (TCP) from one point to another when that movement does not have to be in a straight line

These commands can be used in a RAPID code line as followed:

```
MoveL , [X1Y1,Z1], [v] , Zone , Tool \Wobj := WorkObjectName ;
```

Movement Target Speed Zone Tool Work Object  
 type location

```
MoveJ , [X1Y1,Z1], [v] , Zone , Tool \Wobj := WorkObjectName ;
```

Movement Target Speed Zone Tool Work Object  
 type location

```
MoveC , [X2Y2,Z2], [X1Y1,Z1], [v] , Zone , Tool \Wobj := WorkObjectName ;
```

Movement Circle Target Speed Zone Tool Work Object  
 type Point location

With:

Table 3.5. Components for move commands (ABB, 2004; Raspall, 2013).

Name	Definition
Target Location	Target point the TCP will move to. [mm]
CirclePoint	Extra point, used to define circular path. Circular path is defined by start point, circle point and destination point. [mm]
Speed	Maximum speed the robot will try to reach while making the movement. [mm/s]
Zone	Zone data describes the size of the generated corner path
Tool	Tool gives information on which tool is mounted on the robot. This refers to the tooldata, as defined in the beginning of this chapter.
Work Object	Coordinate system the movements for the robot are defined in. This refers to the WobjData from section 3.2.2: Work object coordinate system

### 3.3 Grasshopper

*Rhinoceros 3D* (often referred to as *Rhino3D*) is a strong 3D modelling software in the field of architecture, engineering, and construction, issued by Robert McNeel & Associates (Robert McNeel & Associates, n.d.) With this software, freeform geometries are possible to create. This software is based on NURBS (Non-Uniform Rational Basis Splines) (Romaniak & Filipowski, 2018)). According to V. (2020) these NURBS are mathematical representations of 3D geometry that can accurately describe any shape, from a simple 2D line, circle, arc, or curve to a very complex free form 3D organic surface or solid. For this research, I worked with *Rhino v7*. this software is compatible with most commercial design, drafting, CAD, prototyping, rendering and illustration programs.

### 3.3.1 Concept

There are different plugin's that can be downloaded for *Rhino v7*. One of these plugin's is Grasshopper. In *Rhino v6* and *Rhino v7*, this plugin is automatically downloaded with the software. Grasshopper is a parametric software that visualizes the created objects through the *Rhino3D* software. In Grasshopper, a programming language is used for the creation of geometries. This is shown on a canvas that represents the working area. Different components can be placed on this canvas and can then be connected via nodes. Two macro-classes are identified: 1) parameters, these contain the information (numbers, vectors, geometries...) and 2) operations such as translation, copy, subdivision, scale... (Costantino et al., 2022). When a parameter is changed, a real time change is shown in the geometry in the *Rhino3D* software. An example of a small grasshopper script is shown in Figure 3.6.

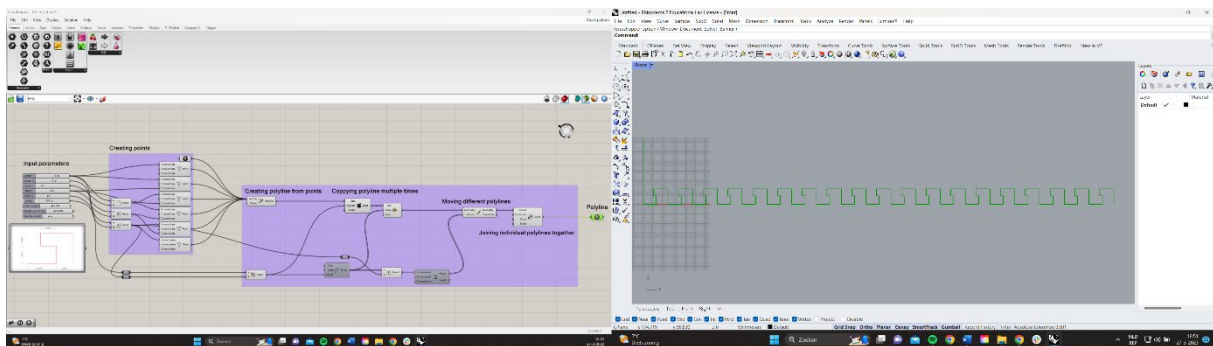


Figure 3.6. Example of 1) Grasshopper on the left 2) real time view of coded geometry in *rhino3D* on the right (Rhino Grasshopper, 2022).

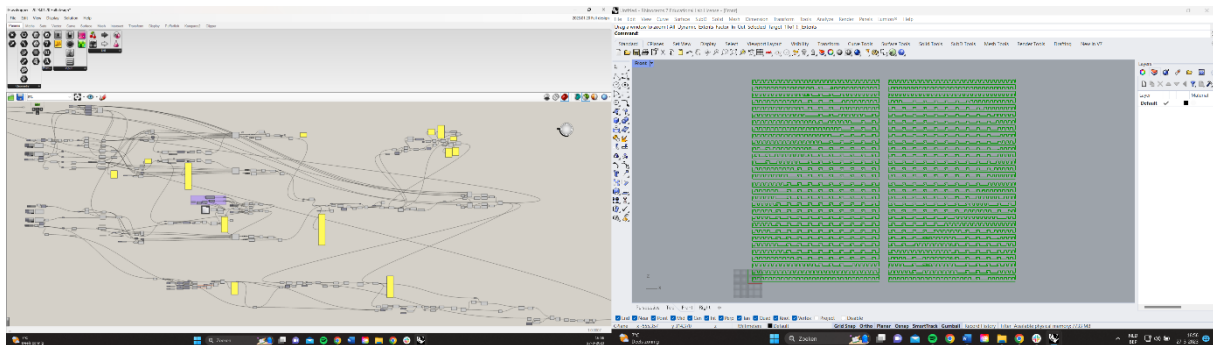


Figure 3.7. Used grasshopper script for phase 4, multi-panel design (Rhino Grasshopper, 2022).

Grasshopper is used to create the different geometries that were used as toolpath for the robotic concrete printer. This toolpath is then translated with HAL robotics plugin for grasshopper to rapid code, as briefly introduced in section 3.2 (“ABB Rapid Code”). Figure 3.7 shows an example of a geometry created in *Rhino Grasshopper* that was used as toolpath for the prototype design that will follow in section 4.4 (“Phase 4: How to fabricate a multi-panel design with the *Greek Key Pattern?*”).

## 4. PRINT TESTS

### 4.1 Phase 1: How to make perforations with concrete printing techniques?

In the first phase of the research, various patterns were examined and evaluated in order to assess the feasibility of creating perforations in 3D concrete printing. These patterns were derived either from independent brainstorming sessions or through the emulation of existing designs. To have an organized categorization of these toolpath techniques, they were classified into three distinct groups: *Horizontal printing*, *Vertical printing* and a *third and fourth category with the incorporation of specialized techniques such as a Pinch valve and Glass optic fiber reinforcement*. A schematic representation of these categories is provided in Figure 4.1.

The first category, *horizontal printing*, pertains toolpath techniques for which the perforated panel will have a horizontal orientation. This involves the extrusion nozzle moving along a horizontal axis while depositing the concrete material, resulting in a panel with uniform thickness.

The second category, *vertical printing*, involves printing perforated panels in a vertical orientation. In this first phase, no complete panels have been printed yet in this category. Only a first layer, indicating its potential for use in the construction of perforated panels.

The third category is a specific category that includes a toolpath technique with the *insertion of a glass optic fiber* within the printed concrete. This approach is made possible using a specially designed nozzle developed at *TU Graz*, which allows for the insertion of glass optic fibers within the concrete material during the printing process.

The last category, a print was tested that used a *pinch valve* on the nozzle. A pinch valve is used to control the flow of the concrete through the nozzle. this pinch valve can open or close the nozzle, enabling the extrusion of material to be started or stopped at specific intervals. This technique was evaluated during the print process creating pauses in the printed line.

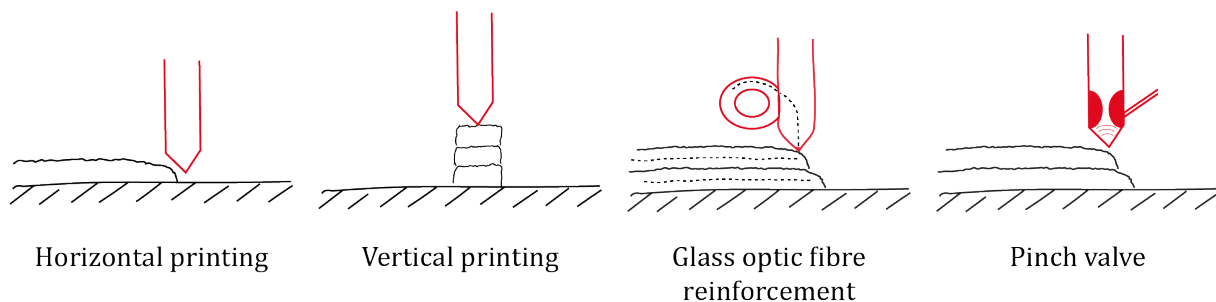


Figure 4.1. Schematic representation of A) Horizontal printing, B) Vertical printing, C) Incorporation of glass optic fibre in print and D) Printing with pinch valve.

### 4.1.1 Horizontal printing

#### **Proposed toolpath techniques for horizontal printing**

Two toolpath techniques covering multiple aspects are presented and evaluated in this category. Both toolpath techniques concern a perforated panel measuring approximately 50cm x 50cm. One toolpath technique represents a regular grid pattern, with the printer following the diagonals of the panel. This toolpath technique will be referred to as the *Horizontal Diagonal Grid*. This way, there is no overlapping within a layer. A second consecutive layer is then printed one layer higher, perpendicular to the first diagonals. A digital representation is made in the CAD software *Rhino3D*, and it's presented in Figure 4.2.

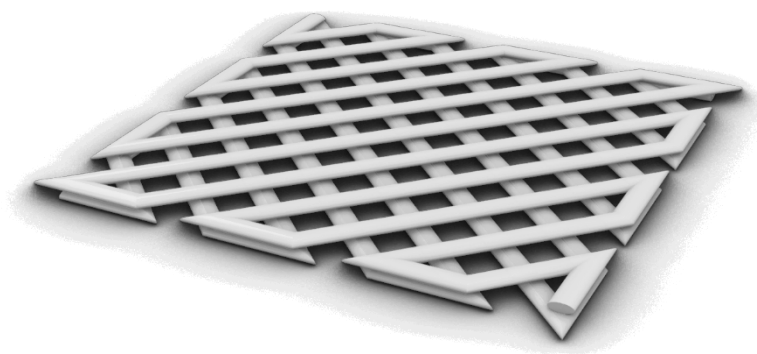


Figure 4.2. 3D model of the Horizontal Diagonal Grid.

The following concept proposed in this category involves the creation of a single-layer panel. The 3D concrete printer moves randomly between different sides of the panel, creating multiple places of overlapping. Another difference in this panel with the previous printed panel is the utilization of an optic fibre network, positioned in a frame. The frame elevates the network 3mm above the print bed and the network is manually tensioned. The maze distance of this network measured 5mm x 5mm, and the panel was printed directly on top of it, with the aim of enabling the concrete material to flow through the mazes of the network. This way, the panel can be held together upon initial cracking by the optic network. Figure 4.3 illustrates a digital model of this proposal, created in *Rhino3D*.

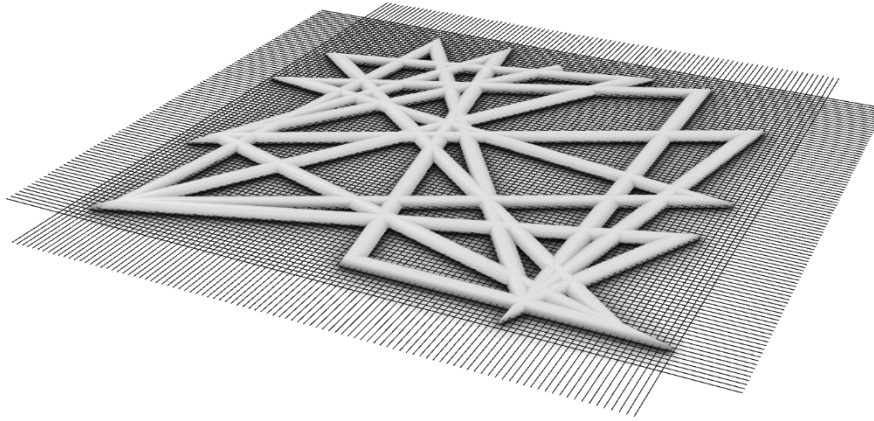


Figure 4.3. 3D model of the Horizontal Glass Optic Fibre Network Panel.

Both toolpath techniques present a suitable technique for creating perforations. The first toolpath technique results in a regular grid of perforations with constant dimensions. For the second toolpath technique, each perforation is different, due to the randomness of the followed toolpath. The glass optic fibre gives extra structure to the print, against cracking.

#### ***Test results for horizontal printing***

Horizontal printing is an ideal printing method for creating perforations. This is because, for horizontal printing, there is a continuous support on the printed material from the print bed, thereby avoiding gravitational issues such as bridging or overhanging. This allows for the creation of perforations that remain open and have a high degree of precision and control. The printed output closely resembles the original design from the digital model created in Rhino3D. The results from these prints are shown in Figure 4.4. Since there are no gravitational problems, the variety in perforations is virtually endless. Both the shape as the size is controllable with the toolpath from the 3D geometry. This allows for variations in both shape and size of the perforations. The category of horizontal printing can produce perforations ranging from relatively small ones, about  $1\text{cm}^2$ , to larger ones up to  $50\text{cm}^2$ . Variations can be made within a printed panel with different shapes and sizes of perforations. Due to the horizontal printing character, a uniform and flat texture is created on the printed lines, without any expressive texture being generated. The amount of material used by these panels is dependent on the resolution of the perforations and typically ranges between  $12\text{kg/m}^2$  to  $40\text{kg/m}^2$ .



Figure 4.4. Printed results of left) Horizontal Diagonal Grid, right) Horizontal Glass Optic Fibre Network Panel showing the opportunities and challenges of creating a horizontal perforated panel with a 3D concrete printer.

**Cracking.** A highly recognizable problem in the horizontal test prints was cracking. This can be seen in Figure 4.5. As water evaporates during hardening, the concrete shrinks, leading to tensile stresses in the concrete sections. Since the printed lines are fixed at some points (print bed, previous layer), they prevent the concrete from shrinking. Tensile stresses will start to build in the concrete sections. The concrete can only withstand a given stress. If the occurring stress gets larger, the concrete will break. This is a reoccurring problem in the horizontal prints, due to the small cross sections of the printed lines (ca. 25mm x 8mm).

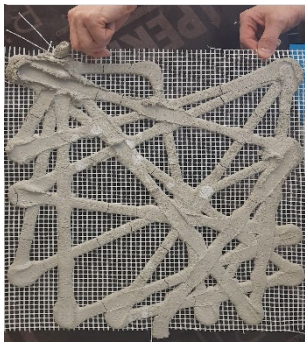


Figure 4.6. Horizontal Glass Optic Fibre Network Panel held together by the fibre network, after cracking.

To address this problem, solutions such as: continuously spraying water evaporation onto the print or covering it with water-resistant foil, can be implemented to slow down the drying process, reducing the likelihood of cracking (Schmidt & Slowik, 2009). In the case of the *horizontal glass optic fibre network panel*, the printed lines still experience cracking in certain areas. However, the fibre network functions to maintain the structural integrity of the concrete by interweaving with the cracks and preventing further separation. Figure 4.6 shows how this panel is kept together by the fibre network, after cracking has occurred.



Figure 4.5. Cracking occurs in the concrete at the weakest points, caused by drying shrinkage and increasing inner stresses.

**Corners.** Excess material build-up in the corners is a common challenge in 3D concrete printing. Figure 4.7 provides a close-up view of a corner on the horizontal glass optic fibre network panel, revealing an excess of material in comparison to non-corner areas, resulting in a knot-like appearance. This phenomenon is caused by the acceleration of the 3D concrete printer, which slows down to zero before changing direction and then accelerates to full speed again. This prolonged time at the corner, in combination with a constant extrusion of material by the printer results in an excessive build-up of material in the corners. One potential solution involves understanding of the relationship between the speed of the robot and the extrusion of the material. Specifically, when the printer slows down, the extrusion rate should decrease correspondingly (and vice versa.).

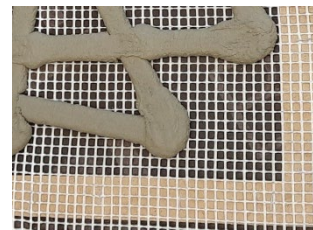


Figure 4.7. excessive material at corners on the Horizontal Glass Optic Fibre Network Panel has a knot-like appearance

**Overlapping.** The *Horizontal Glass Optic Fibre Network Panel* presents a challenge of multiple overlapping regions in the print, leading to excessive material deposition and bulk points, as illustrated in Figure 4.8. This phenomenon occurs due to the thickness of the printed line (ca. 25mm) and can compromise the appearance of the final product. To address this issue, an algorithm must be incorporated to the grasshopper script to avoid multiple overlapping regions and optimize the printing process. By avoiding excessive material deposition and reducing the occurrence of bulk points, the proposed algorithm can improve the quality of the printed panel.

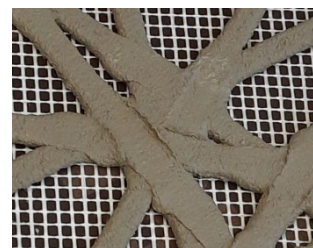


Figure 4.8. Multiple overlapping lines in the panel leads to excessive material deposition, creating bulk points.

**Layer height.** The used layer height influences the cross section of a layer and the adhesion with the previous layer. For a first testprint of the *Horizontal Diagonal Grid*, an erroneous value of 25mm was used for the layer height. The standard layer height, used for the Baunit printer at TU Graz measures approximately 8mm. As a result of this mistake, the printer hovered above the first printed layer, only dropping down the concrete on top of it. A subsequent test print was conducted after this, with the correct layer height parameter of 8mm. Figure 4.9 shows the comparison of these two prints. Notably, in the first scenario, where the concrete is dropped on top of the first layer, the cross-section exhibits a more rounded shape, compared to the second attempt. However, since the concrete is only dropped on top of the first layer, it is not firmly pressed against the underlying layer, leading to cold joints. In the second attempt, the adhesion between the two layers was stronger.



Figure 4.9. A higher layer height (left) results in a rounder cross-section but a weaker intermixing between layers. Layer height of 8mm (right) provides a strong intermixing between layers.

Overall, the horizontal panel has great potential for creating perforations. However, due to its limited thickness of only one layer, it is prone to weak stiffness, resulting in frequent cracking. An attempt to address this issue might be to construct the panel using multiple layers. By doing so, the cross sectional area increases, providing more resistance against tensile forces. This modification may improve the overall strength and durability of the panel, but might also change the overall feel and look of these panels. No test prints however have been done to test this hypothesis.

#### 4.1.2 Vertical printing

##### **Proposed toolpath techniques for vertical printing**

Three toolpath techniques are presented and tested. In this category, the panels are printed vertical, with no support. For these first test, no panels have yet been developed. The proposed toolpath techniques were limited to only a few layers, to avoid collapsing.

**Vertical Zigzag Panel.** The *Vertical Zigzag Panel* focuses on the vertical movements of the 3D concrete printer. During the printing process, the printer will move up and down along the Z-axis, in order to fabricate a zigzag shape. The goal of this toolpath technique is to print a concrete line with varying layer heights within a single line. Next, a second straight line with a consistent layer height can be printed on top of the initial line, to fabricate cavities between the different layer heights. This toolpath technique is visualized in *Rhino3D*, from which the geometry is shown in Figure 4.10. this proposal will be referred to as the Vertical Zigzag Panel.

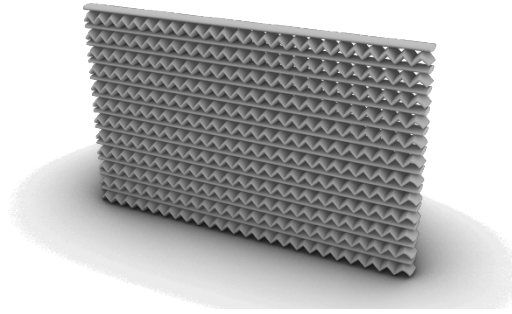


Figure 4.10 .3D model of the Vertical Zigzag Panel.

**Greek Key Panel.** The *Greek Key Panel* also focuses on the vertical movements of the printer. This panel is inspired by a reference project created by Dutch architects, Bekkering Adams, called *Firewall*, shown in Figure 4.11 (StudioAdams, 2017; Teague, 2017; Tissink, 2017). As An attempt to recreate this design, a new shape emerged, referred to as the “*Greek Key*”. This name comes from a geometric repeating motif, often used in Greek and Roman art (Knuff, 2017). An example of this pattern is shown in Figure 4.12 The used toolpath for this panel has a similar shape, hence its name. The objective was to fabricate layered lines, with openings in the panel at the points where the toolpath changes direction, similar to the design of Bekkering Adams Architects. On top of a *Greek Key Line*, a straight line will follow. This proposal is shown as a digital CAD model in Figure 4.13.



Figure 4.11. Bekkering Adams Architects – Fireplace. Reference project for the Greek Key Panel (Bekkering Adams Architecten, 2017).



Figure 4.12. Greek Key, decorative motive form used in Greek and Roman art forms the basis of the Greek Key Pattern (Dreamstime, n.d.).

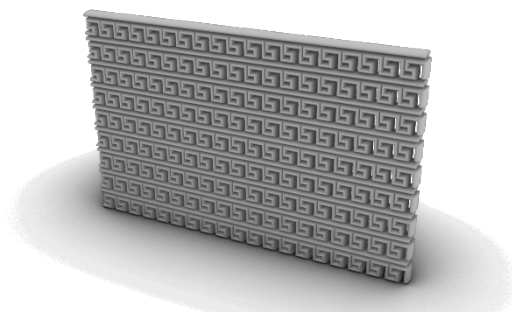


Figure 4.13. 3D model of the *Greek Key Panel*.

**Vertical Crossed Panel.** Another toolpath technique is called *the Vertical Crossed Panel* and is based on the intercrossing of consecutive layers. One layer follows a horizontal zigzag pattern. A subsequent layer on top of this has the same zigzag shape but is mirrored. This creates an intercrossing effect between the layers. These panels will be referred to as *Vertical crossed panels*. The digital model from this is shown in Figure 4.14 the aim is to create small gaps between the

layers at the points where they intercross, as perforations. The mirrored zigzag patterns create open spaces inside the panel. This can be utilized for inserting artificial lighting into the panels.

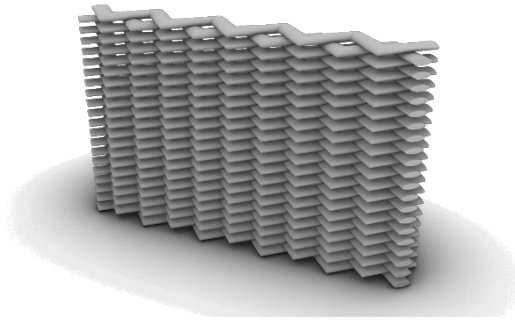


Figure 4.14. 3D model of the Vertical Crossed Panel.

### **Test results for vertical printing**

Vertical printing shows to be a more challenging print strategy to fabricate perforations into a concrete printed panel. This is due to the influence of gravitational forces on the viscous concrete. The lack of support around the perforations results in the bridging or overhanging effect, causing the fluid material to drop down under the influence of gravity. However, test prints have demonstrated that it is possible to fabricate perforations using this strategy. The size of the perforations however is limited due to collapsing once the gravitational forces become too large. Perforations are possible with a size of about  $1 \text{ cm}^2 - 5 \text{ cm}^2$ . The influence of gravitational forces, however, gives a higher degree of unpredictability in the final outcome. The physical models show differences when compared to digital models created in *Rhino3D*. When a single line was printed, cracking occurred on the weakest spots of the lines, with the smallest cross sections. However, once multiple lines were printed into a panel, cracking became limited. The panels have a slim thickness, requiring only a small amount of material,  $40\text{kg/m}^2$  to  $80\text{kg/m}^2$ . A rough texture is generated in these proposals, as well as the possibility for strong variations in width and/or height of the printed lines or panels. These variations enable control over the depth and shape of the texture and allow for diverse patterns of perforations.

**Vertical Zigzag Line.** The *Vertical Zigzag Line* has had two test prints. These results are shown in Figure 4.15. The first attempt resulted in cladding of the concrete to the side, due to the low downward movement of the printer. The second attempt used the same geometry with a 2 mm upward shift. This showed to be a working solution. The used geometry had an amplitude of 10 mm and showed a zigzag every 20 mm. The printed line exhibits variations in width and height for the maximum and minimum amplitude of the toolpath. Where the printer moves down, the concrete is pushed to the sides, resulting in a wider, but low path. When the printer moves up, the path gets smaller and higher. These variations in height were the aim of this proposal. The height difference however is not sufficient to fabricate perforations. A second layer on top of this zigzag



Figure 4.15. Printed results of the vertical zig-zag line. Left) first attempt shows cladding on the sides, right) Vertical zig-zag line, whole geometry moved 2mm up.

line will, due to gravitational forces and viscous characteristics, fill in the height differences, leaving no openings between the layers. A potential solution for this might be to increase the amplitude of the zigzag line, or to increase the frequency of zigzags. No tests have been conducted to test this hypothesis.

**Greek Key Panel.** The *Greek Key Line* showed promising results in creating variations with a 3D concrete printer. Figure 4.16 shows small segments of the results from four different tests. The *Greek Key* creates a line with “knot-shapes”. Figure 4.16 shows, that when the parameters are adjusted, these “knot-shapes” can vary in shape. This is highly promising to create variations in the texture of the panel.

These “knot-shapes” also create great height differences on top of a “knot” and next to a “knot”. A second straight layer will be printed on top of this line, with bridging between the “knot-shapes” as a result.



Figure 4.16. By adjusting the parameters of the *Greek Key Shape*, multiple variations in the outcome are possible.

**Vertical Crossed Panel.** Due to an error in the algorithm of the *Vertical Crossed Panel*, the printer went back from its last point to the first point. This led to destruction of the printed model by the printer. Due to time efficiency, no second attempt of this print has been conducted. For that reason, no visual result can be given. However, the findings for this panel had been noted during the printing process. Where the aim was to create small gaps between the layers at the points where they intercross, the result did not show this. No gaps were created at intercrossings. The open spaces inside the panel were created, but are completely sealed, making it not possible to disperse light. To resolve this problem, one solution might be to print multiple consecutive layers with a same orientation, only mirroring the next layers after two or three layers. This proposal is a potential solution for this specific panel but has never been tested.

#### 4.1.3 Printing with incorporation of specialized techniques

##### **Proposed toolpath techniques with pinch valve**

The proposed toolpath technique in this category was printed with the use of a pinch valve. A pinch valve is used to control the flow of the concrete through the nozzle. With the right commands in the ABB Rapid code, the pinch valve can open or close the nozzle and control the concrete flow at specific intervals. The proposed toolpath technique is similar to the *Vertical Crossed Panel* but uses pauses along the print. Short diagonal lines are printed next to each other, the next layer is again a layer existing from short, printed lines, but mirrored. A digital representation of this *pinch valve panel* is shown in Figure 4.17.

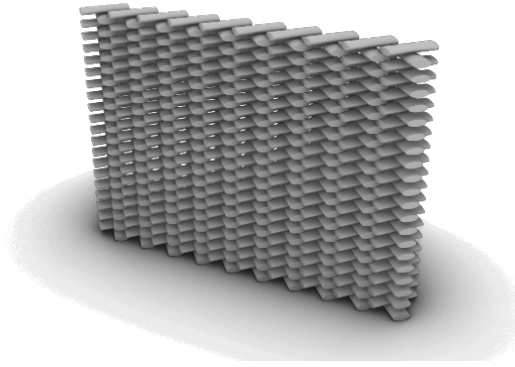


Figure 4.17. 3D model of the Pinch valve panel

### ***Test results with pinch valve***

A pneumatic pinch valve is used to control the flow of concrete in the nozzle. This is generally used to start and stop the extrusion of material at the beginning and end of a print, respectively. In this example, the use of the pinch valve is also utilized to pause concrete extrusion during a print to enable multiple short lines to be printed in one go. A test result of the printed lines is shown in Figure 4.18. Only one layer is printed in this test, to see the effect of the pinch valve. The test results show an irregularity between the movements of the printer and the pinch valve. The pinch valve opens a short while after the printer starts moving, resulting in the beginning of the line not being extruded. The same occurs at the end when the printer decelerates, and the pinch valve does not immediately close, leading to an excess build-up at the end of the line. A better calibration is needed between the pinch valve and the printer to address this issue.

The pinch valve shows a potential to fabricate perforations. However, intensive use of the pinch valve may lead to poor results as the printer is not designed for this purpose. This was told by ir. Robert Schmid, who has worked regularly with the printer and has found this from previous tests with intensive use of the pinch valve. During the test prints for this panel, this problem did not occur. Due to gravitational forces, the size of the perforations will be limited to around  $1\text{cm}^2$  -  $5\text{cm}^2$ . Since the print consists of small individual lines with limited lengths, cracking will not be an issue. By adjusting spacing between lines or the length of the lines, variations can be made in the size of the perforations and the thickness of the panel. This will also result in a rough surface texture with a lot of depth. The panels have a relatively large thickness and will need about  $40\text{kg/m}^2$  to  $70\text{kg/m}^2$ .



Figure 4.18. Printed result of a line, made with the pinch valve.

### ***Proposed toolpath technique with insertion of glass optic fibre***

*Transparent concrete* is a building material with light-transmissive properties. This is due to embedded light optical elements, for example glass optic fibres. Glass optic fibre has as one of its characteristics to transport light because of refraction (Addanki et al., 2018). Light is conducted through these fibres from one end to the other. In order to have a transparent effect, the fibres thus have to go through the whole object. The concept of transparent concrete is first put forward in 2001 by Hungarian architect Aron Losonzi. A first successfully produced transparent concrete block was produced in 2003 under the name LiTraCon (Light Transmitting Concrete) and had large amounts of glass fibre mixed into it. Currently, the largest project that exhibits this technology is an artistic installation, called the 'European Gate' in Hungary (Ranveer et al., 2016; Zielińska & Ciesielski, 2017).



*Figure 4.19. European gate, Hungary, by Aron Lonsoczi and Orsolya Vadasz (Egonis, n.d.).*

Currently, there are not many producers of translucent concrete blocks. Creating these blocks requires specific skills and know how. This makes that these blocks are very expensive, compared to normal concrete, with a price of around €750 for one square meter with a thickness of 2.5cm (Bhushan et al., 2013; Zielińska & Ciesielski, 2017). In this section of the research, an approach is taken to test if it is possible to automate this process, with 3D concrete printing, making it possible to produce more affordable transparent concrete blocks.

At *TU Graz*, a print nozzle was already designed, with the potential to insert reinforcement inside a print. This reinforcement is extruded together with the concrete and is parallel with the toolpath. To fabricate transparent concrete, as described above, the reinforcement however needs to be perpendicular on the panel surface. Therefore, a massive block is designed where the printer always moves perpendicular to the panel. The design of this block is shown in Figure 4.20. Once the concrete is hardened, the sides are cut off, revealing the optic fibre that was inserted. Depending on the thickness of this concrete block, multiple panels can be cut from one block.

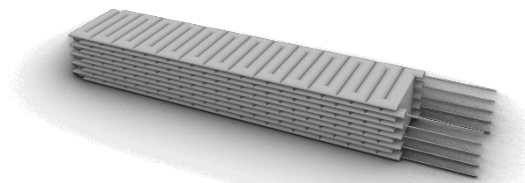


*Figure 4.20. 3D model of the glass optic fibre panel.*

### ***Test results with insertion of glass optic fibre***

During the tests conducted, a large concrete block was printed, which is displayed in Figure 4.21 (left). After one week of drying, this block was cut into panels (right). Depending on the needed thickness of the panels and the thickness of this block, multiple panels can be cut out of it. In this example, two panels were cut out of the block. The sides of the block were rendered unusable as the optic fibre did not completely go through them. This resulted in large amounts of waste material from the sides and hence raises concerns about the efficiency of this proposed toolpath technique. However, increasing the thickness of the block would result in a higher number of panels that can be cut out of this block, while maintaining the same amount of waste material. Nonetheless, as the thickness of the block increases, the hardening time also increases. Therefore, an optimum balance must be found between the thickness of the block and the hardening time.



Figure 4.21. Printed result of glass optic fibre panel.

This printed panel is a massive piece of concrete with a weight of  $1850 \text{ kg/m}^3$ . This will be approximately  $50 \text{ kg/m}^2$  for a panel of 25mm thickness. No perforations are created for this proposal. Light is emitted through optic fibre inside of the concrete. When it is light, the glass optic fibres are hardly visible. Once it gets dark, and there is light emitting on the other side of the panel, all the optic fibres become clearly visible, as they emit the light through the panel. This difference between light and dark is clearly shown in Figure 4.22. The optic fibres are spaced equally, corresponding to a layer height and width of 8mm and 25mm, respectively. The constant grid formation of the optic fibres is a result of the fibres being placed in the centre of the extruded concrete, making it impossible to generate patterns. There are relatively little glass fibres in the concrete, compared to examples from commercial players in this field (e.g., LiTraCon, Lucon, Lucem Lichbeton). Further research may focus on developing a print nozzle that can insert multiple fibres simultaneously to increase the number of optic fibres. Since the panels are cut from one massive brick, the surface has a very smooth, uniform texture.

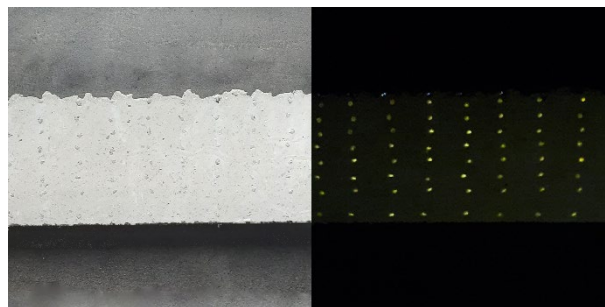


Figure 4.22. Glass optic fibre panel, contrast between light and dark.

#### ***4.1.4 Conclusion***

The first phase of this research has involved the proposal and exploration of multiple toolpath techniques to fabricate perforations with a 3D concrete printer. This has led to different successful

toolpath techniques. Categorized into four categories: *Horizontal printing*, *Vertical printing*, *printing with a Pinch valve* and *printing with insertion of Glass optic fibre*. Table 4.1 presents a comparison of the most crucial characteristics of each category. To achieve the objectives of this thesis, a careful consideration is necessary in selecting the most suitable toolpath technique for further testing.

Vertical printing is considered the most appropriate category for achieving the objectives of this research. Despite the difficulties associated with creating perforations due to gravitational forces, efforts will be made to optimize one pattern from this category in fabricating and controlling perforations. Small perforations are most suitable for creating a privacy barrier, while allowing for natural light penetration through the panel. The rough texture of the panel also creates a distinct aesthetic. Variations in the panels can be achieved by altering the shape of the layers and the perforation size and location. The needed material to fabricate panels is between  $40\text{kg/m}^2$  and  $80\text{kg/m}^2$ . A further ecological approach will be followed to find the ecological impact of this. However, cracking may pose a challenge, but can be mitigated with adequate knowledge.

The *Greek Key Panel* appears to have the most potential in this category due to the large height differences and the ability to modify shape, making it a promising area for further research in continuous pursuit of this project.

Table 4.1. Comparison of different print categories.

	Horizontal	Vertical	Pinch valve	Glass fibre	optic fibre
Possible to make perforations?	Easy	Hard: Viscous material	Hard: Viscous material	/	
Type of perforations	$1\text{cm}^2 - 50\text{cm}^2$	$1\text{cm}^2 - 5\text{cm}^2$	$5\text{cm}^2 - 10\text{cm}^2$	Glass Fibre	Optic
Variations possible	Perforations	Texture Perforations	Texture Perforations	Not possible	
Cracking	Likely	Avoidable	No	No	
Amount of material	$12\text{kg/m}^2 - 40\text{kg/m}^2$	$40\text{kg/m}^2 - 80\text{kg/m}^2$	$40\text{kg/m}^2 - 70\text{kg/m}^2$	$50\text{kg/m}^2$	
Texture	Flat	Rough	Rough	Uniform	

## 4.2 Phase 2: How to control the *Greek Key Shape* with different parameters?

Fundamental differences are observed between the physical output and the digital input. The printer's outcome is characterized by a high degree of uncertainty. The digital input is given to the



Figure 4.23. Toolpath followed by the 3D concrete printer, to fabricate a *Greek Key Line*.

printer as a toolpath. A toolpath is defined as a sequence of instructions that define the movement of a tool on a machine, in this case the print nozzle. It describes the path the print nozzle will follow, while extruding concrete. It includes information about the nozzle's position, speed, and direction at each point along the path (GRZ Software, n.d.). The toolpath behind the *Greek Key* is shown in Figure 4.23.

Several parameters can be used to describe the toolpath for a singular *Greek Key Shape*. To effectively control the printer's outcome, a comprehensive analysis of these parameters and their respective influences is necessary. Figure 4.24 provides an overview of the parameters employed to control the shape in question.

#### 4.2.1 Orientation

**Horizontal Greek Key.** The orientation of the *Greek Key* appears to show a significant impact on the outcome. Although *Phase 1* established that vertical printing is the most suitable for achieving the desired objectives, three test prints were conducted for which the orientation of the *Greek Key* was changed to horizontal. Figure 4.25 and Figure 4.26 presents the parameters and toolpath used in these examples, along with the corresponding results. The initial test print exhibited only small perforations. In subsequent prints, the parameters were doubled, in order to generate larger perforations. From the PLC, the extrusions speed can be controlled. For the first test print, this was set to 30Hz. However, in the second print, where the parameters were doubled, the material extrusion speed was incorrectly set to 35Hz. Another test print was then conducted with the same

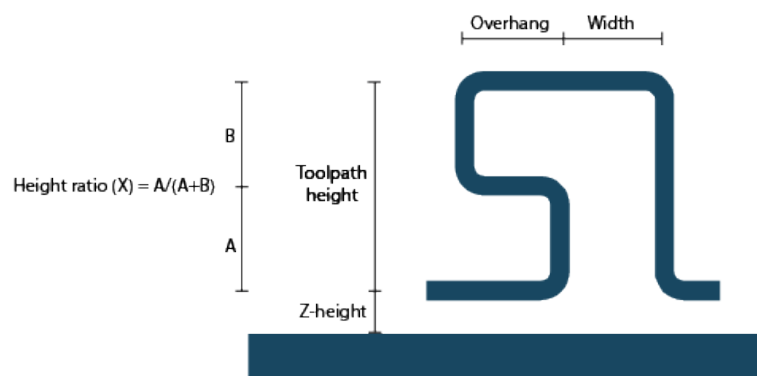


Figure 4.24. Different parameters used to describe the *Greek Key Shape*.

parameters as before, but with the extrusion speed set to 30Hz. Less material resulted in larger perforations. The outcome differed completely from the *Greek Key* printed vertical. Although both options exhibited perforations, that can both be varied, it was concluded in Section 4.1 ("Phase 1: How to make perforations with concrete printing techniques?") that horizontal printing is not the optimal choice for achieving the objectives. Horizontal printing resulted in a flat texture that lacked variation. Moreover, the panels exhibited low tensile strength and were prone to cracking when subjected to movement, making them suitable only for small panels. Therefore, this research will focus exclusively on vertical printing of the *Greek Key*.

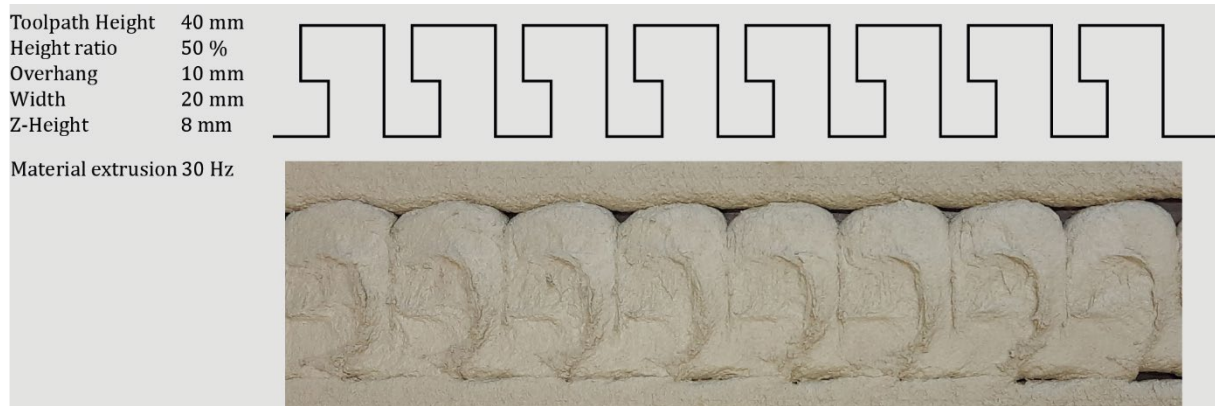


Figure 4.25. A horizontal printed *Greek Key Pattern* results in a completely different result. Perforations are still obtained.

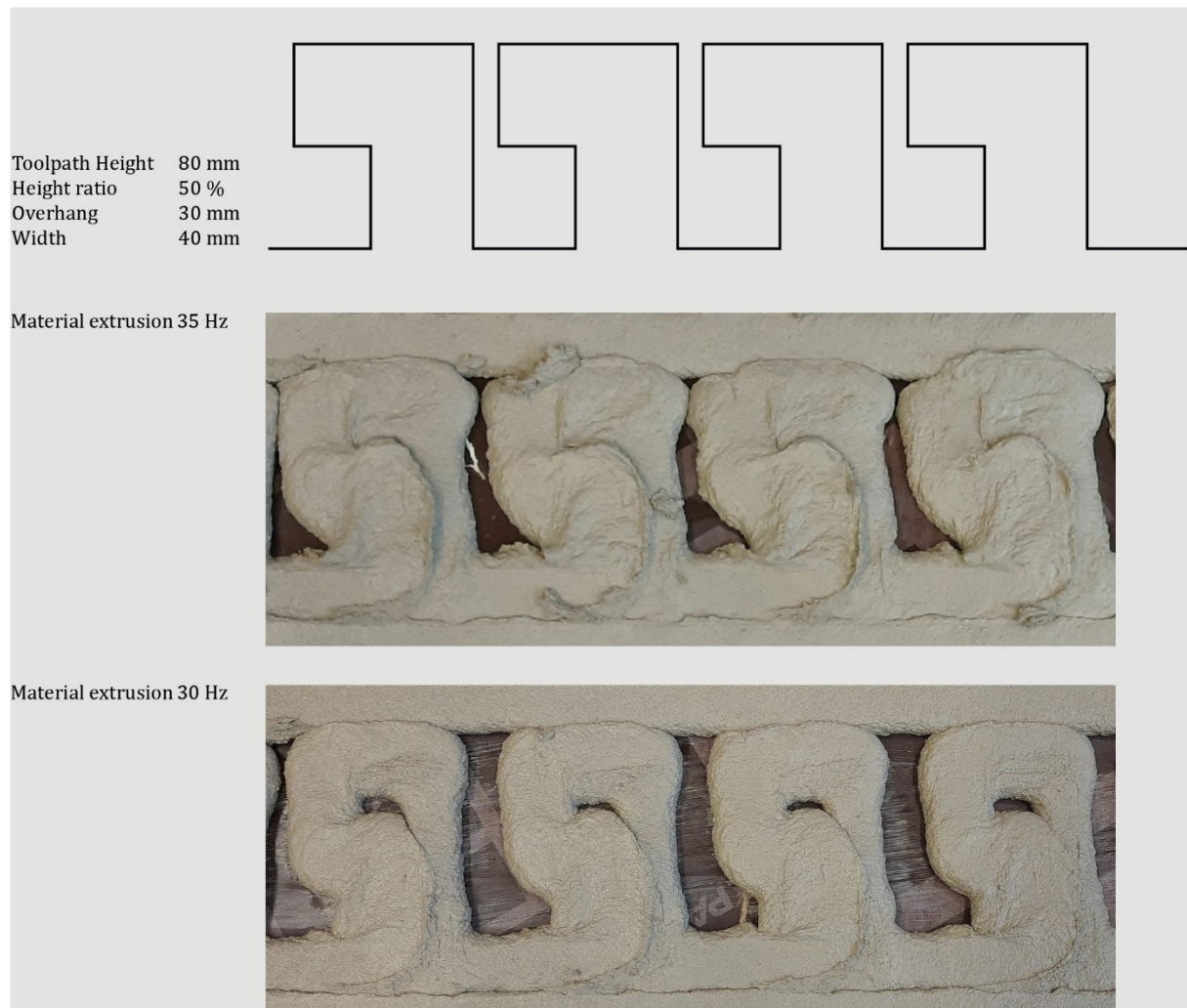


Figure 4.26. doubling of the *Greek Key* defining parameters results in larger perforations. Decreasing the material leads to bigger perforations.

**Mirrored Greek Key.** When the *Greek Key* is mirrored, a different result appears from the printer. A small test line was extruded to compare the outcomes. Overall, the shape remained the same, but the scale changed. The test line, shown in Figure 4.27, highlights that the total height differs from that of the original oriented *Greek Key*. Reversing the *Greek Key*, resulted in a significantly

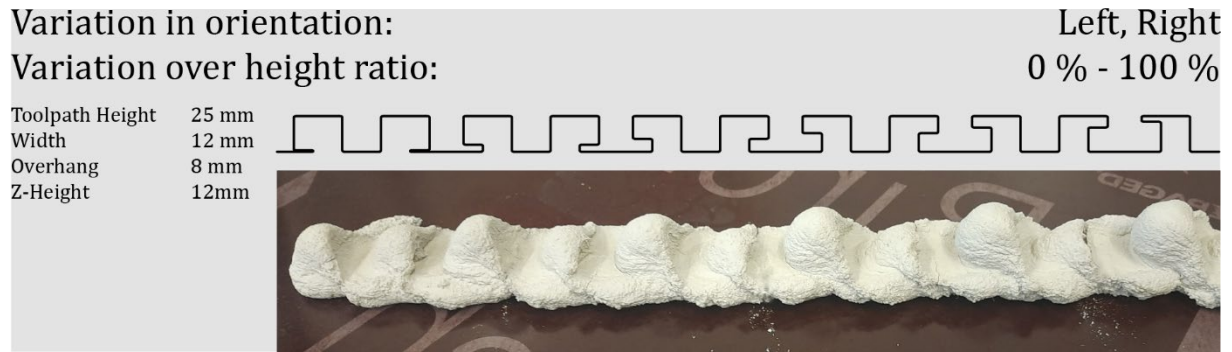


Figure 4.27. Varied, reversed and straight *Greek Key* with an iteration over the height ratio show height differences in the physical outcome.

smaller physical height. Table 4.2 provides measurements of the height for each *Greek Key*. With a color-coded scale ranging from light blue to dark blue indicating the lowest to highest values. When plotted on a graph (Figure 4.28), the differences between the reversed and straight *Greek Key* become clear. At low height ratios, the physical height appears similar for both examples. However, as the height ratio increases, the difference between the two *Greek Keys* becomes more pronounced, reaching up to 12mm. Notably, the graph reveals an inverse relationship: the *Straight Greek Key* increases in height with a higher height ratio, whereas the *Reversed Greek Key* decreases.

Table 4.2 Height of straight and mirrored *Greek Keys* in relation to their height ratio. Color code, ranging from light blue to darker blue indicates lowest to highest values.

Height ratio	Straight	Reversed
0.04	27.71	26.66
0.2	31.75	26.46
0.36	33.01	25.48
0.52	34.76	24.32
0.68	35.33	23.75
0.84	35.85	23.26

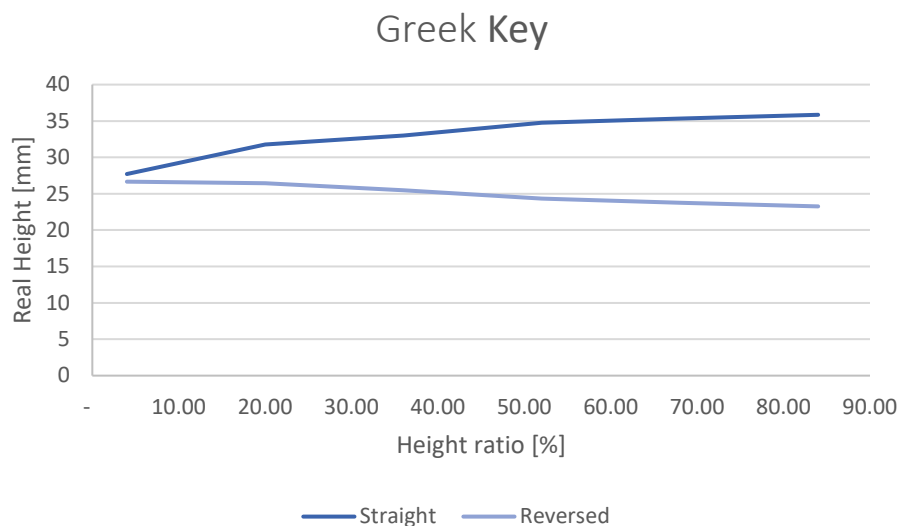


Figure 4.28. Relation between the physical height and the digital height ratio of straight and reversed *Greek Key* show an inverse relationship.

#### 4.2.2 Moon shape vs. round shape vs. leaning shape

Over the course of various tests, two distinct shapes have been observed in the *Greek Key*: a *round shape* and a *moon shape*. These shapes were determined through printed test lines that exhibited a gradual change either in the height ratio, or a combination of increasing overhang and decreasing width. Figure 4.29 illustrates the specific toolpaths and their parameters used in these tests. The tests itself are shown in Figure 4.30. The first three lines (1, 2, 3) show a gradual change in the height ratio from 0% to 100%, with different toolpath heights of 40mm, 24mm and 16mm.

The next three lines (4, 5, 6) exhibit a gradual change increase in overhang from 0 mm to 28 mm on one side and a gradual decrease in width from 30 mm to 2 mm on the other side. These lines vary in height ratio, with values of 25%, 50% and 75%, respectively. The toolpath height is 20mm for the three.



Figure 4.29. Used toolpaths and parameters for iterative parameterisation of the *Greek Key Shape*.

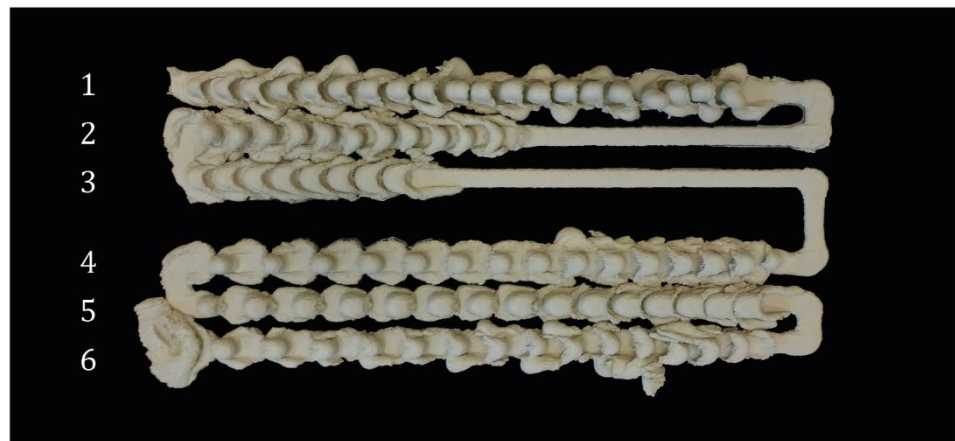
All six of these described lines were printed simultaneously. The initial attempt (A.) utilized an extrusion speed of 35Hz, resulting in *Greek Keys* with excessive material pushed to the sides. To mitigate this issue, the extrusion speed was reduced to 27Hz for the subsequent prints (B., C.), resulting in more consistent *Greek Keys*, with less built-up material. Another attempt to fabricate slinker printed lines with minimal excessive material, was to raise the entire geometry. The previous test prints were printed at a Z-height of 8 mm, the standard value for the used print-setup. In the last test prints (C.), the Z-height was increased to 12 mm.

Print A. and B. showed some excessive build-up material, leading to more unpredictable outcomes. Since the focus of this research is to control the *Greek Key*, the majority of this analysis will focus on the print C. with a material extrusion speed of 27Hz and a Z-height of 12mm. Nevertheless, in

A.  
Material extrusion 35 Hz  
Z-height 8 mm



B.  
Material extrusion 27 Hz  
Z-height 8 mm



C.  
Material extrusion 27 Hz  
Z-height 12 mm

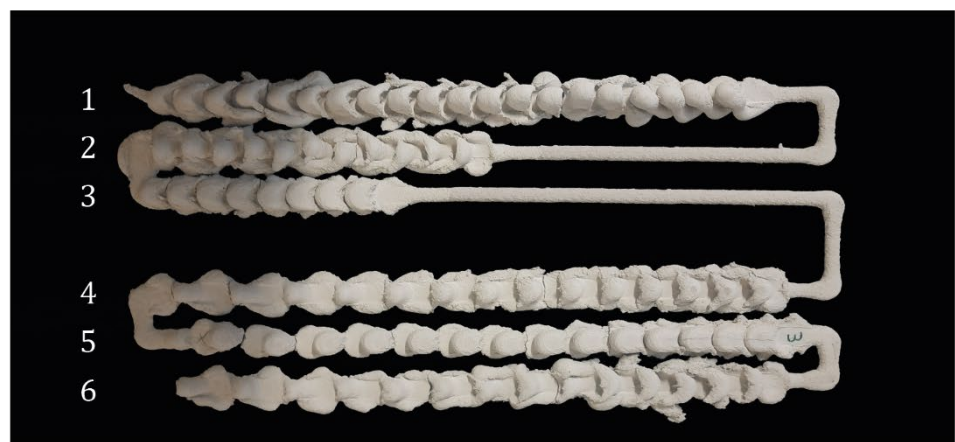
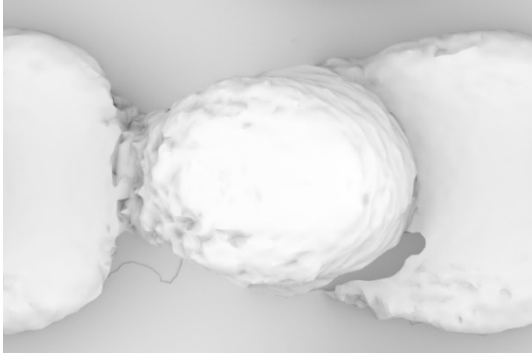
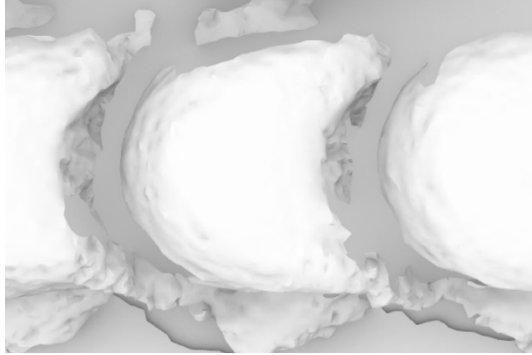
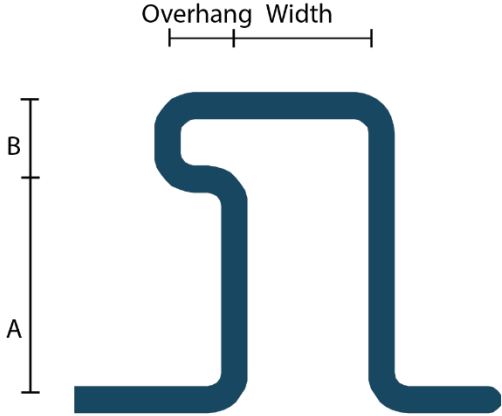
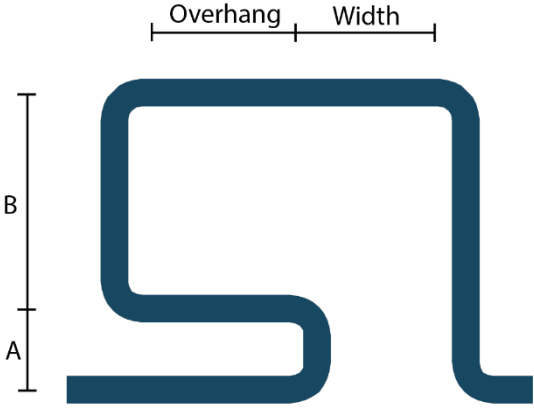


Figure 4.30. Printed concrete lines with gradual change over parameters show different shapes as outcome.

all the prints, two main shapes are recognized in the *Greek Keys*: a *round shape* and a *moon shape*, named after their respective forms. Both shapes are detailed in Table 4.3.

. In order to achieve a *round shape*, the *Greek Key* must be described with a high height ratio and a small overhang. Conversely, the *moon shape* is derived from a *Greek Key* with a small height ratio and a large overhang. Parameters in between produce iterations between these two shapes. The convex form of the *moon shape* is a consequence of the printer nozzle descending into the viscous concrete and leaving its imprint. The convex shape will thus always show the same diameter. The toolpath height parameter does not impact the shape of the *Greek Key*; it solely influences the height of the shape. A higher toolpath height corresponds to a greater physical height, and vice versa.

Table 4.3. Two distinct shapes are recognized in the test prints of the *Greek Key*.

	
	
<p><b>Round shape</b></p> <ul style="list-style-type: none"> <li>- Height ratio ↗</li> <li>- Overhang ↘</li> </ul>	<p><b>Moon shape</b></p> <ul style="list-style-type: none"> <li>- Height ratio ↘</li> <li>- Overhang ↗</li> </ul>

**Leaning shape.** Apart from the *round shape* and *moon shape*, another distinct shape has been recognized, which only manifested in the last test print (C.). This particular shape, referred to as the *Leaning shape*, only showed with specific parameters as illustrated in Figure 4.31. An attempt was made to reproduce this shape in a new print by duplicating the parameters. The shape was recognizable again, as depicted in Figure 4.32, but it exhibited some uncontrollable behaviour wherein certain shapes leaned more to the side than others. This shape introduced significant

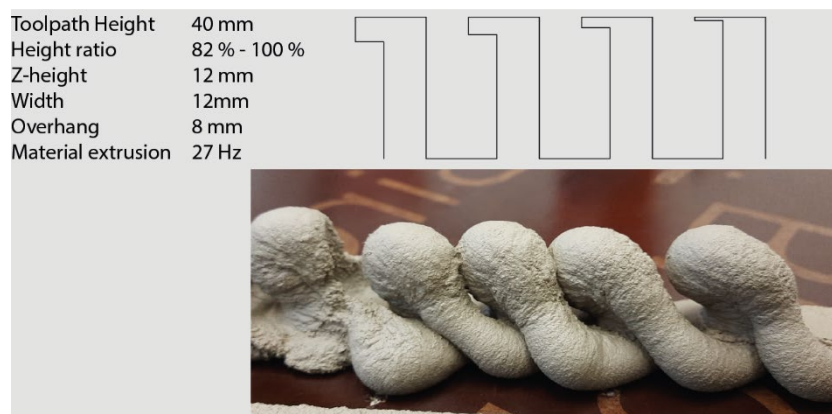


Figure 4.31. Specific parameters resulted in a new shape, the Leaning shape.

uncertainties, which would pose problems when used in a multi-layered panel, as these uncertainties would cumulate with each other and lead to failure.



Figure 4.32. Attempt on recreating Leaning shape leads to uncontrolled shapes.

#### 4.2.3 Width variations

Several iteration lines of the *Greek Key* were printed with a gradual change over the width, resulting in results as *uncontrolled falling down*, *folded extrusion* and *bridging*. Four different lines were printed, each featuring a gradual change in the width of the *Greek Key*. The toolpaths that have led to these prints are shown in Figure 4.33. To conduct a detailed analysis, a 3D scan was performed on these test prints, providing an overview shown in Figure 4.34. In the following discussion, more specific problems and findings of these prints are described. Indicated by a red square on Figure 4.34.

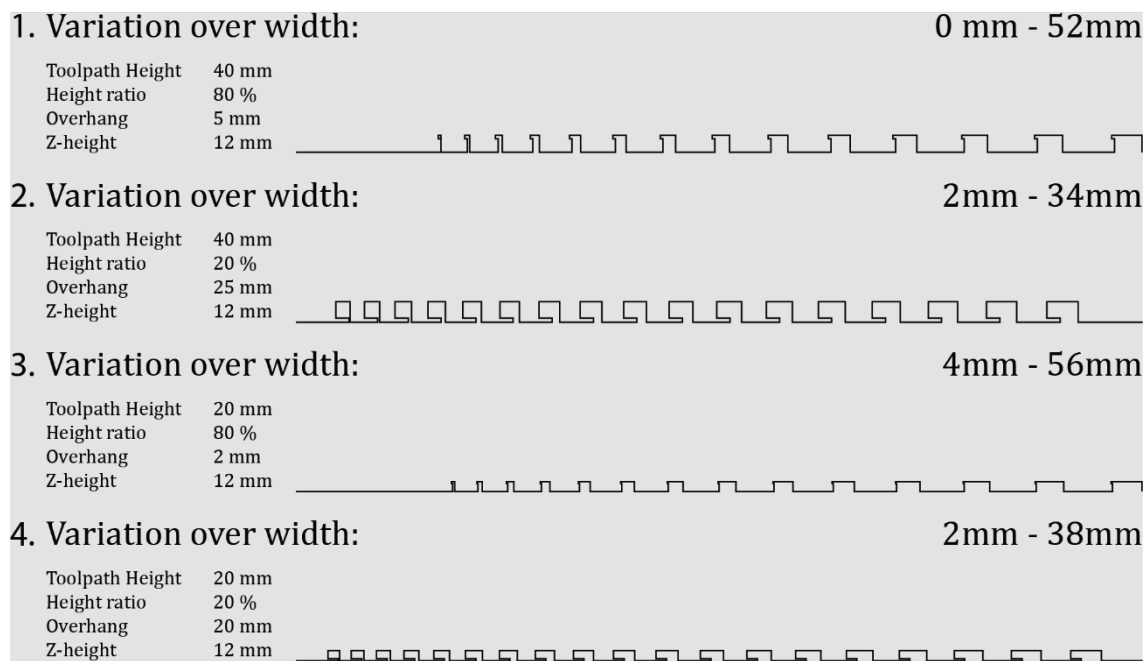


Figure 4.33. Toolpaths and parameters of the *Greek Key* with a variation over the width parameter.



Consequently, when the printer moves downward again, it pulls the concrete along, causing bridging. To avoid cracking in the prints, it is crucial to prevent this phenomenon and thus limit the width of the *Greek Key* to a maximum of 36mm.

#### 4.2.4 Toolpath height and real height

The toolpath height differs from the real height. A function will give the relation between both values. An analysis was conducted on the concrete lines “1”, “2” and “3” of print “C.” from 4.2.2 (“Moon shape vs. round shape vs. leaning shape.”), shown in Figure 4.30 and printed with a material extrusion of 27Hz and a Z-height of 12mm. The analysis focused on the first three lines (1, 2, 3), which were printed with a variation over the height ratio and a toolpath height of either 40mm, 24mm or 16mm. Each individual *Greek Key* was measured and compared with the corresponding toolpath height in function of its height ratio. The results are presented in Table 4.4 and are graphically depicted in Figure 4.39.

Table 4.4. Relation between the toolpath height and the real height, in function of the height ratio. A color-code, ranging from light blue to darker blue indicates the lowest to the highest values.

Height Ratio	Toolpath Height	Real Height	Height Ratio	Toolpath Height	Real Height
2.5	40	29.9	4.166667	24	31
7.5	40	34.3	12.5	24	30.1
12.5	40	35.2	20.833333	24	30
17.5	40	39.8	29.166667	24	31.4
22.5	40	36.5	37.5	24	31
27.5	40	37.4	45.833333	24	30.3
32.5	40	40	54.166667	24	33.5
37.5	40	40.9	62.5	24	33.6
42.5	40	42.7	70.833333	24	33.5
47.5	40	43.2	79.166667	24	32.8
52.5	40	44.5	87.5	24	33.7
57.5	40	44.4			
62.5	40	43.9	Height Ratio	Toolpath Height	Real Height
67.5	40	45.8	6.25	16	28.4
72.5	40	46.7	18.75	16	28.4
77.5	40	48.2	31.25	16	28.3
82.5	40	46.1	43.75	16	28.5
87.5	40	46.6	56.25	16	28.4
92.5	40	45.2	68.75	16	28.5
97.5	40	46.9	81.25	16	28.4
			93.75	16	28.2

A colour gradient, ranging from light blue to dark blue, indicates the values from low to high. The *Greek Key Shapes* show an increasing real height as the height ratio increases. At a height ratio of 0%, all *Greek Keys* have a real height of approximately 28mm-30mm, regardless of their toolpath height. As the height ratio starts to increase, the real height also increases. For a higher toolpath height, the increase in real height will grow faster compared to lower toolpath heights. However, a greater variation and unpredictability is measured in their real height for *Greek Key Shapes* with

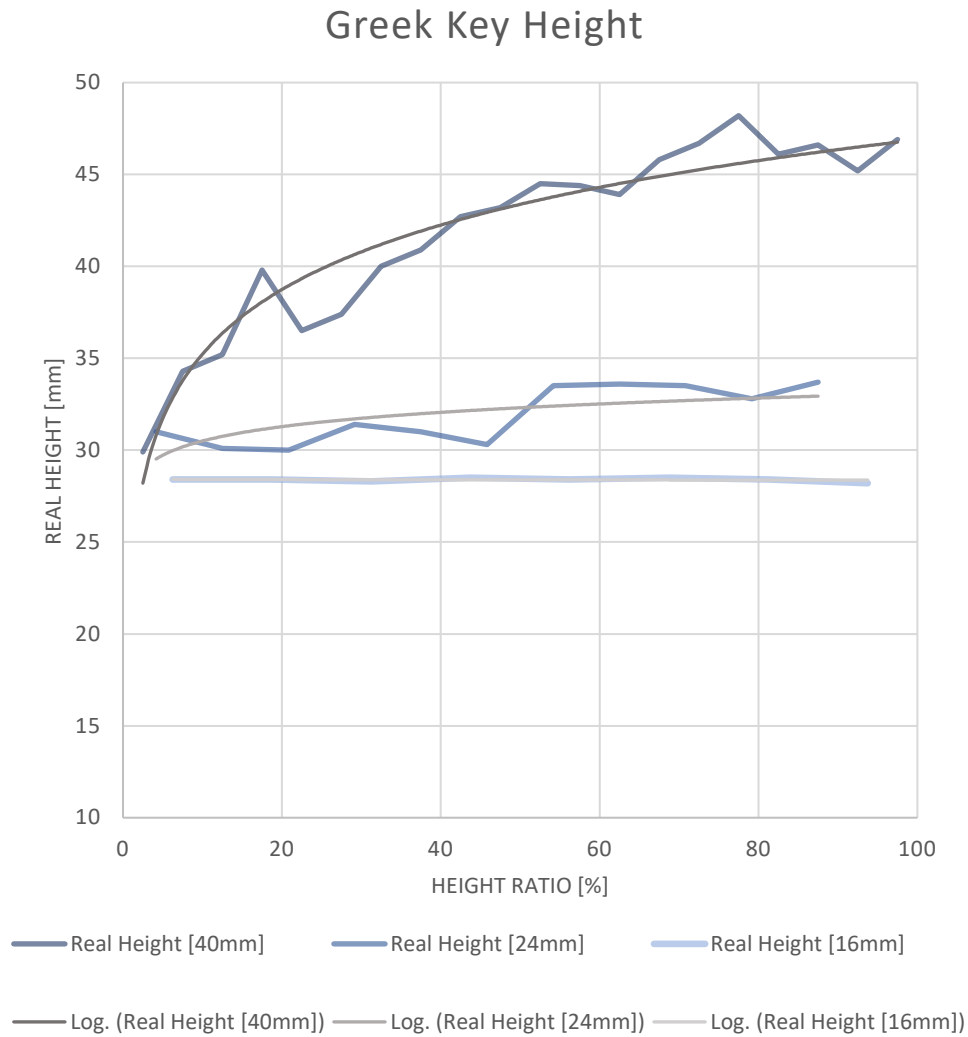


Figure 4.39. The real height is shown in function of the height ratio for a *Greek Key* with toolpath height 40mm, 24mm and 16mm. A logarithmic trendline approaches these values.

a larger toolpath height. The real height of the highest *Greek Keys* shows a large variation, while the lowest *Greek Keys* maintain relatively constant values. The real height does not align closely with the toolpath height.

From the data plotted in Figure 4.39, a logarithmic relationship is recognized in the values. Using *Microsoft Excel*, logarithmic trendlines were derived to fit the data. The derived functions are in the form:

$$H = A \ln(x) + B \quad \text{eq. 4.1}$$

With

$H$  = Real height [mm]

$x$  = Height ratio [%]

The trendlines are derived as follows:

Table 4.5. logarithmic trendlines give an estimation of the real height for a given toolpath height and height ratio.

Toolpath height	Logarithmic trendline	
40 mm	$H = 5,0648 * \ln(x) + 23,563$	eq. 4.2
24mm	$H = 1,1235 * \ln(x) + 27,912$	eq. 4.3
16 mm	$H = -0,015 * \ln(x) + 28,443$	eq. 4.4

A relation must be defined for the A and B values. From further analysis, A is found to follow a linear relationship with the toolpath height and can be described as:

$$A = 0,22h - 3,7 \quad \text{eq. 4.5}$$

The B value can be defined as a second-degree polynomial:

$$B = -0,008h^2 + 0,276h + 26 \quad \text{eq. 4.6}$$

With:

$h$  = Toolpath height [mm]

Combining these formulas yields a function for the real height ( $H$ ) in terms of the toolpath height ( $h$ ) and the height ratio ( $x$ ):

$$H = (0,22h - 3,7) * \ln(x) + (-0.008h^2 + 0,276h + 26) \quad \text{eq. 4.7}$$

And can be inversed to solve for  $h$  as:

$$h = 13,75 * \ln(x) - \sqrt{3025 \ln^2(x) + 190 \ln(x) - 2000H + 56761} + 17,25 \quad \text{eq. 4.8}$$

**Limitations.** This formula provides a good estimation of the real height. However, Figure 4.39 demonstrates there is always some degree of unpredictability in the height. The actual outcome may deviate from the result of this function. Furthermore, this equation is only applicable to *Greek Key Shapes* with a constant width of 12mm and overhang of 8mm. Altering these parameters would yield different real height results. Additionally, the formula assumes a Z-height of 12mm and a material extrusion of 27Hz, as these were the specific parameters used to derive this formula. Additionally, it is crucial to consider the hardware characteristics involved in the experiment. Different hardware components, such as the robotic arm, seventh axis, printhead and nozzle, cement type and other, can influence the results as well. Due to time management, these limitations were not known during all the phases of the research, for which this formula was sometimes wrongfully used, for *Greek Keys* with other parameters.

#### 4.2.5 Straight layer

A second layer is printed on top of a *Greek Key Line*. This is a straight line, following the standard 3D concrete printing methodology. This layer serves as the base for a consecutive *Greek Key Line*, in order to build a panel out of this pattern. To ensure adequate intermixing and preservation of the perforations, the straight line is extruded at a specific height above the *Greek Key*.

For the tests, a *Greek Key Line* is printed with a toolpath height ( $h$ ) of 20mm and a height ratio ( $x$ ) of 75%. Based on equation 4.8, the estimated real height of this *Greek Key Line* is 31,34 mm. A second straight line is printed on top at a Z-height of 33mm, 37mm and 41mm, as Shown in Figure 4.40.

In all three tests, there is observable intermixing between the layers. A Z-height, 2mm above the estimated real height (Z-height = 33mm) appears to be filling the gaps between the *Greek Key Shapes*, resulting in minimal perforations. A test with 6 mm difference (Z-height = 37mm) show larger perforations, However, the best results are achieved with a Z-height 10mm above the real height of the *Greek Key*. This value of 10mm will be used in the continuation of this research to fabricate multi layered panels with the *Greek Key Shape*.

Z-Height 33 mm



Z-Height 37mm



Z-Height 41 mm



Figure 4.40. Z-height of straight line influences the perforation area of the *Greek Key*.

#### 4.2.6 *Greek Key Component*

In order to generate *Greek Key Geometries* in *Rhino Grasshopper*, a custom component was created using a Python script. This node takes the parameters described earlier as input and produces *Greek Key Geometries* as output (see Figure 4.41). The Python script begins by defining each individual vertex of the *Greek Key*, based on the provided input parameters. These vertices are then connected to form a polyline, which represents the outline of the *Greek Key*. Finally, the geometry is translated to the specified start point, aligning it properly within the desired context.

By connecting lists or data trees to the various inputs of the Grasshopper node, the script can produce multiple instances of the *Greek Key*, each with its own unique set of parameters. This capability enables the design of different variations within the context of the *Greek Key Pattern*.

**Height formula.** The height formula is applied in *Rhino Grasshopper* by sequentially executing specific mathematical commands within the Grasshopper environment. To streamline this process and enhance the script's readability, all these commands are encapsulated within a cluster component, as depicted in Figure 4.42. This node requires two inputs: the "Real height ( $H$ )" and the "Height ratio ( $x$ )" parameters. By providing these inputs, the cluster component calculates and outputs the toolpath height ( $h$ ). Placing this cluster component before the *Greek Key Component* ensures that the calculated toolpath height can be utilized as the input for the ToolpathHeight parameter in the *Greek Key Component*.



### 4.3 Phase 3: How to control the perforations?

#### 4.3.1 Arc panel

An arc-shaped panel was printed with a constant *Greek Key Pattern*. The *Greek Key* used in this panel had a width of 28mm and an overhang of 2mm. A toolpath height was set to 20mm with a height ratio of 75%. The real height of this *Greek Key* was measured from previous test, and does not rely on the height formula (eq. 4.8). Figure 4.43 demonstrates the result of this print. The arc shape of the panel was chosen in order to gain stability. In this panel, between two *Greek Key Layers*, the printer printed two straight layers. This was done to recalibrate the base layer for the *Greek Key* and to eliminate imperfections from the previous *Greek Key Layer*. Consequently, each consecutive *Greek Key Layer* had to be mirrored to the previous one. This showed to be working well. However, further steps will test if it is possible to achieve successful results with only one straight layer.



Figure 4.43. Arc shaped panel shows rough texture and perforations that transmit light.

**Texture.** For a multi-layered panel, the texture is formed by material falling down to the sides. An alternating pattern is created between a *Greek Key Shape* and a falling slab of concrete, as shown in Figure 4.44. This hanging slab is a result of the downward movement of the *Greek Key*, where the printer produces surplus material that is then pushed aside. Despite the identical definition of each *Greek Key*, slight differences were observed in the final outcome, indicating a degree of unpredictability in the printer's outcome.



Figure 4.44. Alternating pattern between *Greek Key* and hanging slab fabricates a rough texture.

**Initial layer.** On the arc-shaped panel, the first layer is a *Greek Key Line*. Since this layer is printed on top of the print bed, there is no space for the extruded surplus material to fall to the sides, resulting in a distinct texture compared to other layers. Further tests will commence with a straight line as the initial layer, followed by a *Greek Key Line* where surplus material can fall to the sides, aiming to achieve a homogenous texture.

#### 4.3.2 Toolpath vs. physical results

The *Greek Key Pattern* is defined by a toolpath that follows a specific pattern. Expectations would be that the 3D concrete printer would produce results similar to this toolpath. However, the shapes and panels generated exhibit significant differences from the toolpath. Predicting the precise appearance of the printed result based solely on the toolpath is challenging. Despite the clear pattern depicted by the toolpath, the extruded concrete takes the form of a line with small "knots" (cfr. The *Greek Key*). Subsequent layers are printed on top of these "knots", bridging between them while slightly sagging downwards. A visual comparison between the toolpath and the physical outcome is given in Figure 4.45.

The inconsistencies between the toolpath and the physical outcome primarily stem from the characteristics of the viscous material during extrusion and the influence of gravity on this material, as well as the movements of the printer moving and pushing the concrete aside. As a result, sagging, kneading, and deformation occur on the concrete, leading to a shape that deviates from the defined toolpaths. Therefore, understanding the generation and the control of the *Greek Key Pattern* becomes crucial in this context. Some level of control has been achieved in this

research, though full control is not possible. Each *Greek Key* varies from others, regardless of the parameters used.

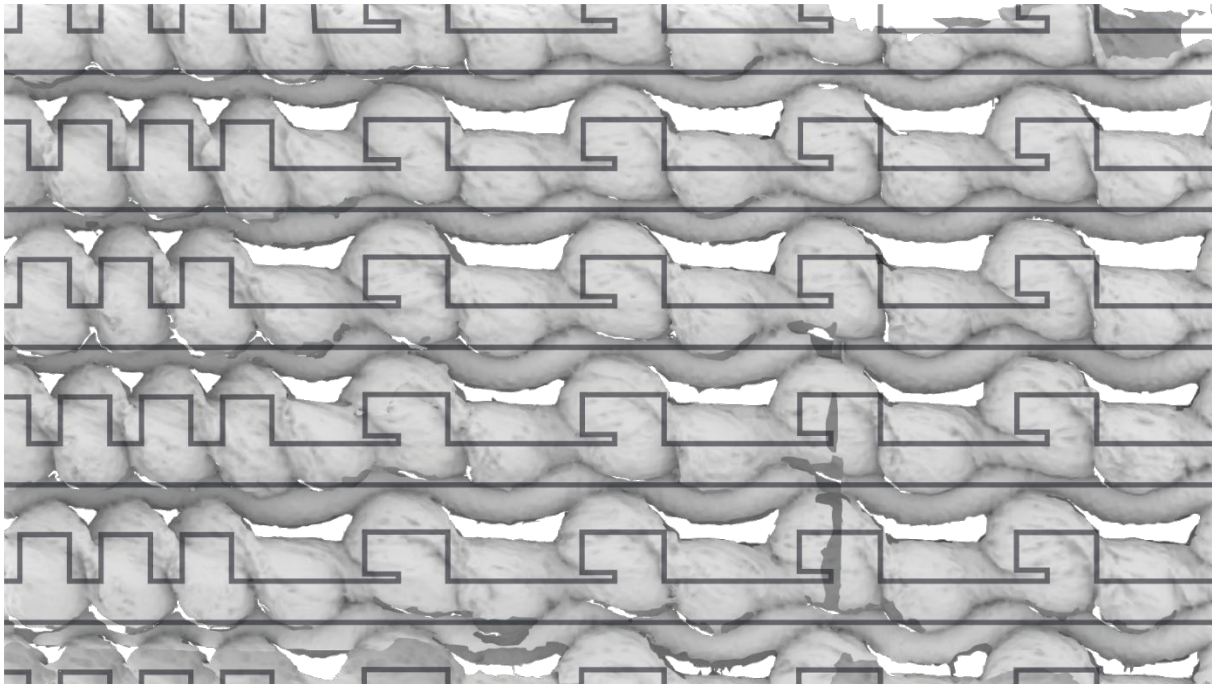


Figure 4.45. Toolpath and physical print show inconsistencies. An unpredictable outcome is generated from this toolpath.

### 4.3.3 Perforation parameters

Design criteria for the perforations were determined based on three panels, each measuring approximate 500mm x 500mm. Figure 4.46 illustrates these panels along with the corresponding toolpaths. The variations used in the panels are specified in Table 4.6. For the panels varying in layer height and inter width, *Greek Key Shapes* were used with a width of 12mm and an overhang of 8mm. The height formula (eq. 4.8) allowed for these shapes to estimate the real height, used in the design of these panels. The printed panels each show a failure on the left upper corners. This problem is caused by a malfunctioning side support design, not by the variations in the perforations.

Table 4.6. Different values create variations in the perforations, used in Figure 4.46.

	Varying layer height	Varying inter width	Varying shape
From	$h = 15 \text{ mm}$	c.t.c. = 22 mm	Moon shape - Overhang 8.5mm - Height ratio 20%
To	$h = 35 \text{ mm}$	c.t.c. = 50 mm	Round shape - Overhang 0mm - Height ratio 100%

**Layer height.** A gradual change over the toolpath height creates variations in the height of the perforation. Decreasing the toolpath height leads to smaller perforations. Moreover, at the lowest toolpath height in this panel (15mm), consecutive layers fill the perforations, resulting in no openings. The panels did not exhibit any failure due to the increasing height parameter, except on the highest layer with a toolpath height of 35mm. It is unclear whether this failure was caused by the failing side support or the *Greek Key Shape* being unsuitable for a toolpath height of 35mm.

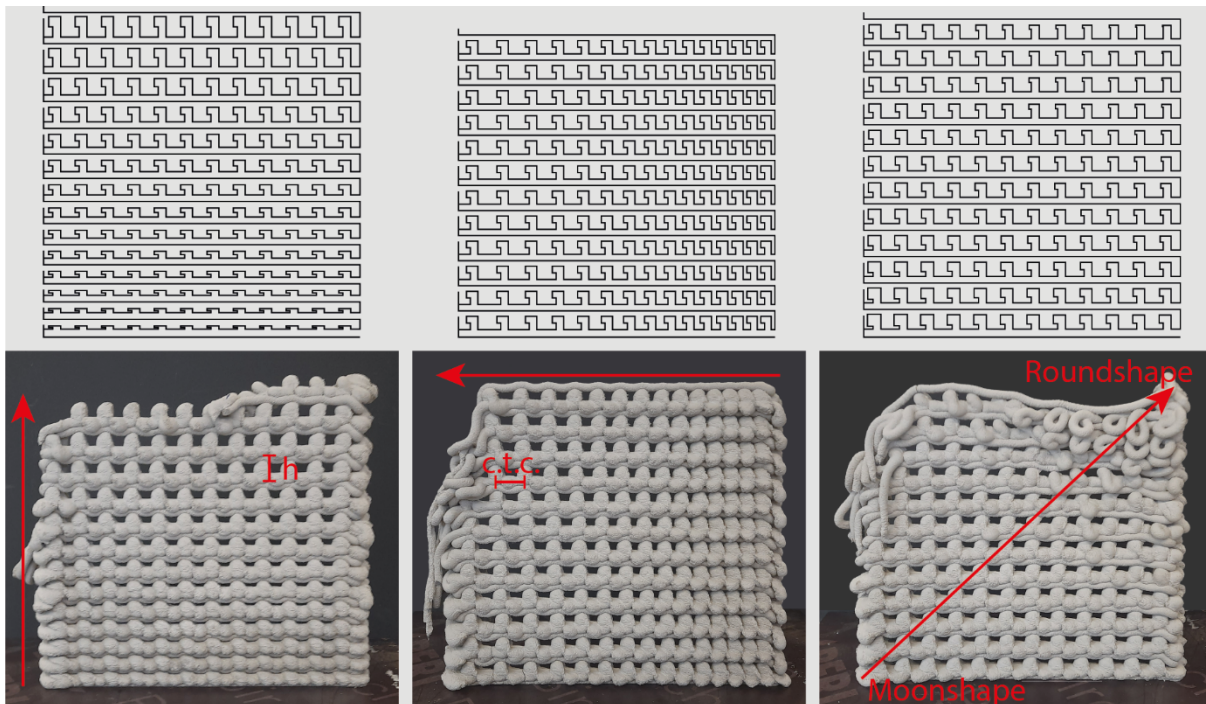


Figure 4.46. Panels show variations in parameters as real height, centre to centre distance and shape variation. Failure is recognized for too large parameters.

However, a toolpath height of 35mm thus seems to define the limit. Cut-out samples from this panel also revealed that the top layers (highest toolpath heights) easily break off, indicating insufficient intermixing of these layers. The straight layer must obtain a reduced Z-height to create better intermixing.

**Centre-to-centre distance.** The centre-to-centre distance (c.t.c. distance) between two *Greek Key Shapes* determines the width of the perforation. In this panel, where the used *Greek Key Shapes* have a width of approximately 12mm, a minimum centre-to-centre distance of 22mm results in approximately 4 mm of perforation, leaving almost no perforation. The largest perforations in this panel, at a c.t.c. distance of 50mm, measures about 26 mm. No failure was observed due to the increasing c.t.c. distance, indicating that no limit value had been crossed. However, it should be noted that a larger c.t.c. distance reduces the number of *Greek Keys*, resulting in fewer contact points between layers. This will reduce the mechanical strength of the panel.

**Shape.** Variations in the shape of the *Greek Key* did not seem to have a significant impact on the overall texture and look of the perforated panel. Only upon close observation inside the perforations, differences between a *moon shape* and a *round shape* were noticeable. Therefore, the overall variations in the perforation patterns mainly arise from the centre-to-centre distance and the layer heights. The height formula was applied to this panel as well; however, due to a changing overhang parameter of the *Greek Key*, the height formula did not always result in working results. Failure has occurred in the top corner of this panel due to incorrect use of the height formula and decreasing of the overhang parameter to 0, which lead to uncontrolled falling of the *Greek Key Shapes*, which caused errors in consecutive layers. To avoid collapsing, it is best to maintain the overhang and width parameters at 8mm and 12mm, respectively, as demonstrated in the examples from section 4.2.4 (“Toolpath height and real height”), This approach ensures better control over the shapes since this research provides a more elaborated analysis for these specific parameters.

**Alternating pattern.** The *Greek Key* can be executed in either a continuous pattern where each consecutive *Greek Key Layer* places the *Greek Key Shapes* on top of each other, maintaining alignment without any shift or displacement, or in an alternating pattern where the *Greek Key* is replicated in consecutive layers with a slight shift or displacement, as depicted in *Figure 4.47*. Consequently, this creates either a visually distinct and staggered arrangement or a uniform and continuous appearance of the *Greek Key Pattern* on the printed panel.



*Figure 4.47.* Alternating *Greek Key Pattern* creates a staggered arrangement.

**Straight layer.** Two straight lines in between two consecutive *Greek Key Layers* resulted in failure. *Figure 4.48* illustrates the collapse of a test panel printed with this configuration. Previous panels only incorporated one straight layer between two *Greek Key Layers*, which proved to be adequate in eliminating imperfections from the previous *Greek Key Layer* and providing a suitable base for printing a new *Greek Key Layer*. However, it should be noted that a double straight layer does not necessarily lead to panel failure. The successful printing of the arc-shaped panel, presented in *Figure 4.43* demonstrates that such a configuration can be achieved successfully.



*Figure 4.48.* Double straight layer leads to failure of the panel.

**Perforation ratio.** Depending on the c.t.c. distance and the layer height, different sizes of perforations can be achieved. The perforation ratio, denoted as the ratio of perforated area to panel area (eq. 4.9) quantifies the degree of perforation.

$$\text{Perforation ratio} = \frac{\text{Perforated area}}{\text{Panel area}} \quad \text{eq. 4.9}$$

To assess the impact of layer height variation and c.t.c. distance on the perforation ratio, measurements are conducted and visually presented alongside the corresponding panels, as depicted in *Figure 4.49*. Although the data available is currently insufficient to establish a precise mathematical relationship between either the toolpath height and the perforation ratio or between the c.t.c. distance and the perforation ratio, a quasi-linear trend is observed.

For small c.t.c. distances or toolpath heights, the perforation ratio tends to decrease, possibly reaching 0%. Conversely, as the values of c.t.c. distance and/or toolpath height increase, the perforation ratio exhibits a corresponding increase. With a maximum measured c.t.c. distance of approximately 47mm, a perforation of around 15.3% is obtained. Similarly, by increasing the toolpath height up to 25mm, the perforation ratio increases up to approximately 18.4%. It is important to note that the size of the perforation is constrained by the maximum values of the c.t.c. distance and layer height. However, no specific maximum parameters have been applied in these tests, suggesting that the measured maximum perforation ratio of 18.4% may not yet represent the upper limit.

**Light transmission.** The perforation ratio also serves as a valuable indicator of the light transmission capabilities of the panels. In a simplified scenario where reflection of the incident light is neglected, the transmitted natural light can be calculated by eq. 4.10, multiplying the incident light by the perforation ratio to estimate the amount of natural lighting penetrating through a given panel or façade.

$$\text{Transmitted light} = \text{Incident light} * \frac{\text{Perforated area}}{\text{Panel area}} \quad \text{eq. 4.10}$$

Thus, the perforation ratio not only quantifies the extent of perforation but also serves as an approximate ratio for evaluating the light penetration of a panel.

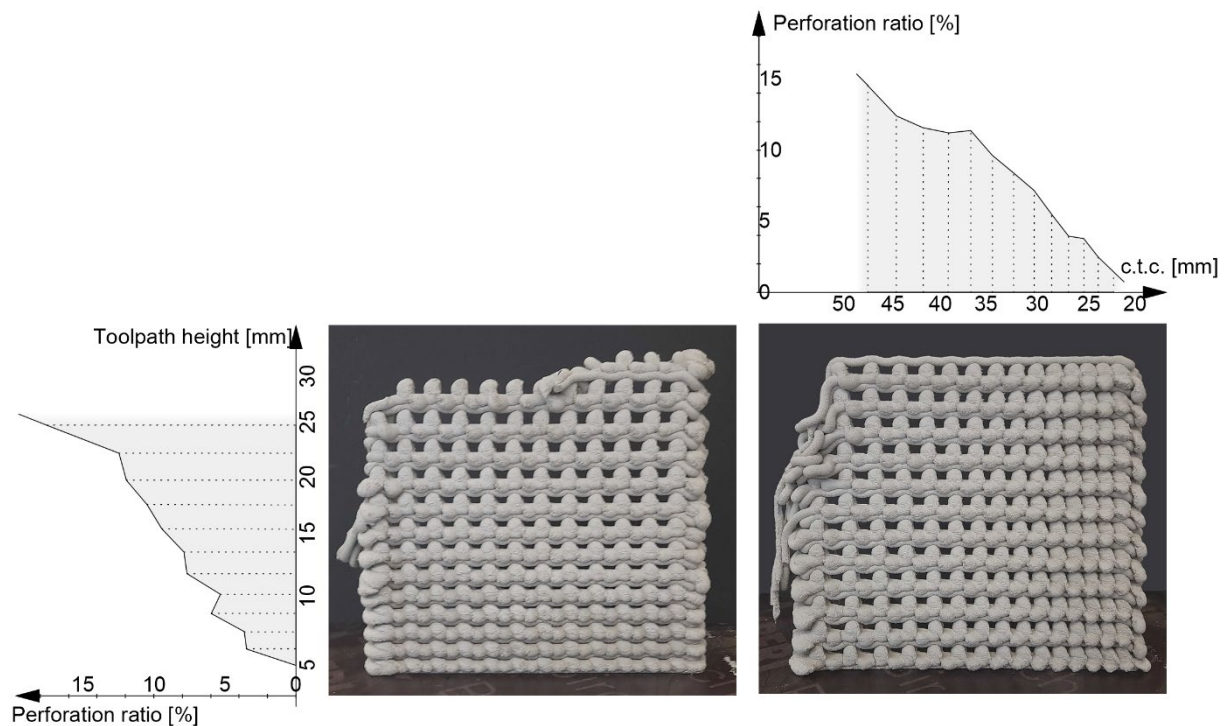


Figure 4.49. Increasing toolpath height or c.t.c. distance show a quasi-linear growth with the perforation ratio.

#### 4.3.4 Side support

To ensure the stability of a rectangular panel during and after printing, side support is necessary. Initial tests were conducted without any support, which resulted in the panel falling over after several layers.

**Greek Key based support.** A first type of side support that was tested utilized the *Greek Key Shapes*, as depicted in Figure 4.50. The used *Greek Key Shapes* had no overhang and a close c.t.c. distance, resulting in a solid structure with almost no perforations. The *Greek Keys* were designed to have a similar height to the panel's layers. However, failure occurred on the left support side, as seen in Figure 4.50 (right) The toolpath that results in this side support is illustrated in Figure 4.52. The toolpath's outermost line on the left side exhibited only a minor upward movement, as this connected the straight layer to the *Greek Key Layer*. This resulted in less material being deposited at this specific spot. Consequently, the area at this spot was lower than that of the *Greek Key Shapes*. Therefore, subsequent layers also printed this area lower than the other *Greek Keys*. This cumulative error ultimately led to failure. On the right side, the toolpath's outermost line had a longer vertical trajectory, controversy connecting the *Greek Key Line* to the straight line. This provided more material at that area. Therefore, this side had sufficient support and remained intact. Since the failure of the side support affected the overall panel results, an improved side support structure is required.



Figure 4.50. Greek Key based support: left side shows cumulative failure, right side provides support.

**Straight line based support.** A side support, based on the traditional 3D concrete method with a layer-wise built, proved to be a solution for side structure, as shown in Figure 4.51. The toolpath for this side structure is presented in Figure 4.52 Depending on the layer height of the *Greek Key Layer*, the side will consist of four or six layers to match the height of the straight line and the *Greek*

*Key Line.* The printer is capable of printing layer heights approximately ranging from 6mm to 12mm. An algorithm is implemented in the Grasshopper code that uses the height equation to derive an estimated real height from a given toolpath height. This value is on its turn divided in an even number (four or six) of layers between 6-12mm. However, each layer will likely have different layer heights. Resulting in either thicker or thinner layers and making the side support not completely homogeneous. A smaller layer height will result in a wider layer and vice versa. This small error does not significantly impact the overall result. Calibrating the printer's speed with the layer height may offer a potential solution to this issue but requires careful calibration. To initiate the *Greek Key Layer* at the bottom, on the left side, a downward movement is necessary. However, this movement causes excess material to accumulate and to be pushed aside at this point, leading to a messy corner.

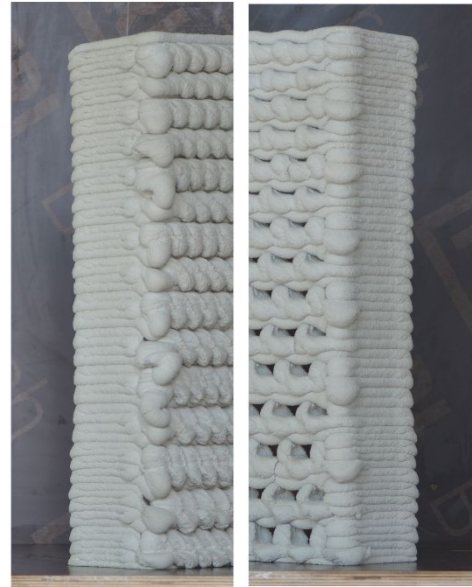


Figure 4.51. Straight line base side support, left corner is sloppy due to excess material, sides show inconsistent widths.

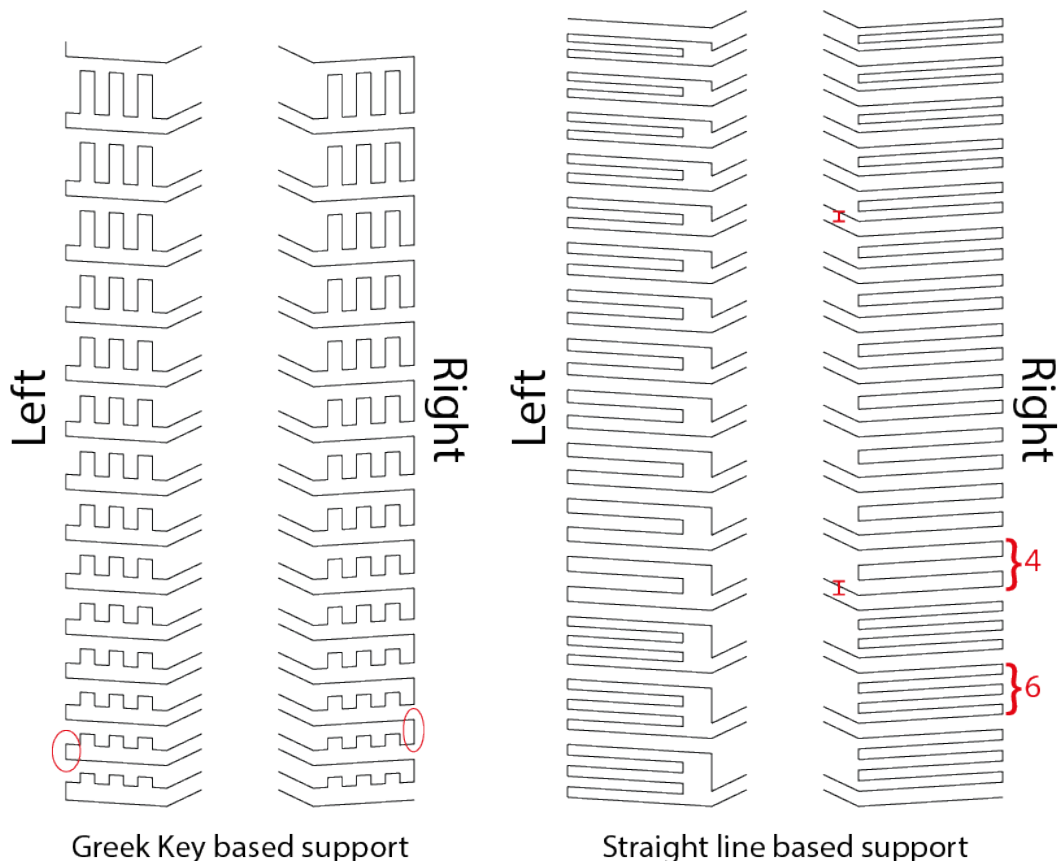


Figure 4.52. Left) Toolpath used for the *Greek Key* based side support, with a small upward movement on the left side, resulting in failure. Right) Toolpath used for the straight line based support, with either four or six layers between each *Greek Key Layer*. Differences in layer height will cause small imperfections in the side support.

## 4.4 Phase 4: How to fabricate a multi-panel design with the *Greek Key* Pattern?

### 4.4.1 Multi-panel design

In a four-panel design, the new form language of the *Greek Key* is tested. A Grasshopper script is developed to determine if a point is inside or outside a geometry, depicted in Figure 4.53. Two different configurations are defined and summarized in Table 4.7. For points inside the oval geometries, a variable *Greek Key Shape* is added, transitioning from a *moon shape Greek Key* in the bottom left corner to a *round shape Greek Key* in the top right corner. The overhang ranges from 12mm to 0mm, and the height ratio varies from 0% to 100%. The c.t.c. distance is constant at 52,5 mm and the *Greek Key Shapes* follow a continuous pattern. For points outside the geometries, a constant *Greek Key Shape* is added with no overhang and a constant width of 12mm arranged in an alternating pattern with a c.t.c. distance of 19,7 mm. The real height for all *Greek Keys* is constant at 23mm. The adhering toolpath height is calculated using the height equation (eq. 4.8). This design incorporates both a gradual change over the *Greek Key Shapes* inside the ovals and an abrupt change in shape, c.t.c. distance, and pattern at the borders of the ovals. All the *Greek Key Shapes* within each panel are connected, resulting in four toolpaths creating a design pattern, as illustrated in Figure 4.54.

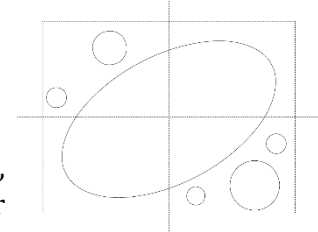


Figure 4.53. Geometry used in Grasshopper code to create a design with the *Greek Key*.

Table 4.7. Used *Greek Key* parameters in the script for a multi-panel design.

	INSIDE OVAL	OUTSIDE OVAL
OVERHANG	Varying: 12mm - 0mm	0 mm
HEIGHT RATIO	Varying: 0% - 100%	n/a
WIDTH	12 mm	12 mm
REAL HEIGHT	23 mm	23 mm
CENTER TO CENTER DISTANCE	52,5 mm	19,7 mm
PATTERN	Continuous pattern	Alternating pattern

During the printing process of the described panels, several were encountered, resulting in failures in some cases and necessitating improvements in others. The final results of the prints can be seen in Figure 4.55. The prints for panel "A" and "D" were successful, meeting the desired objectives. However, panel "B" experienced small errors that escalated into failure in the top layers. Panel "C" presented larger design errors, due to which no final result was achieved for this panel, as it always collapsed before completion. Unfortunately, due to time restrictions, no adjustments could be made to the failed panels for further testing.

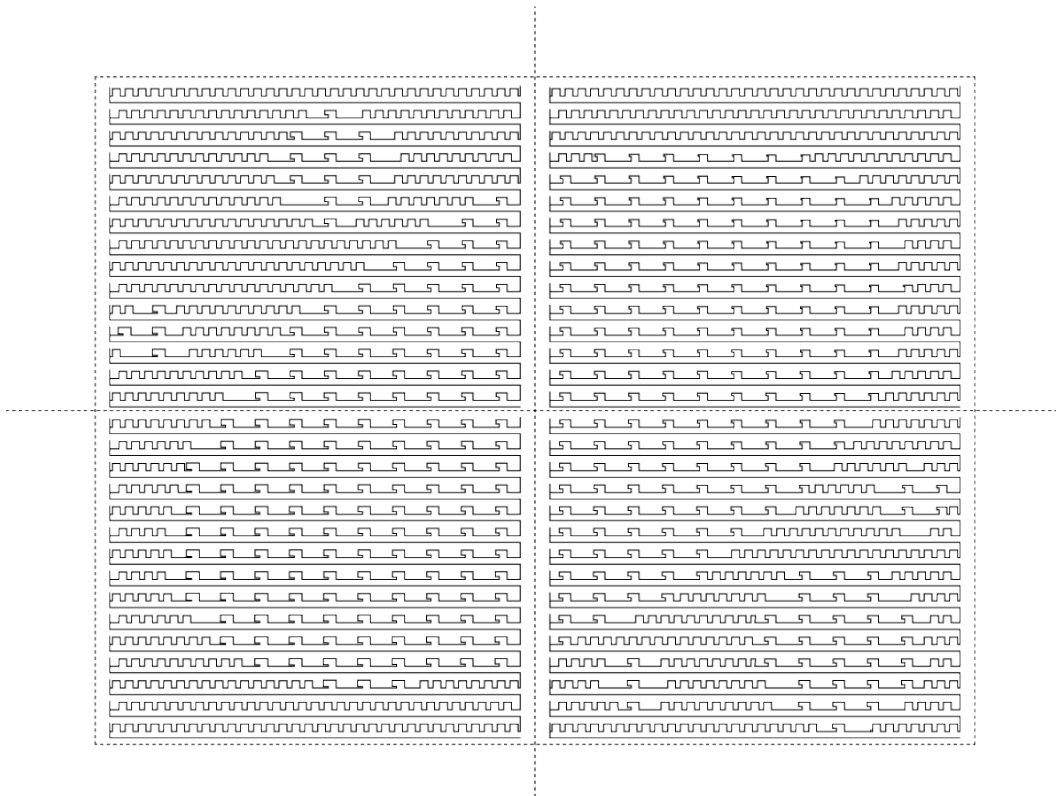


Figure 4.54. Four different toolpaths resulting in the printing of a multi-panel prototype design with the *Greek Key Pattern*.

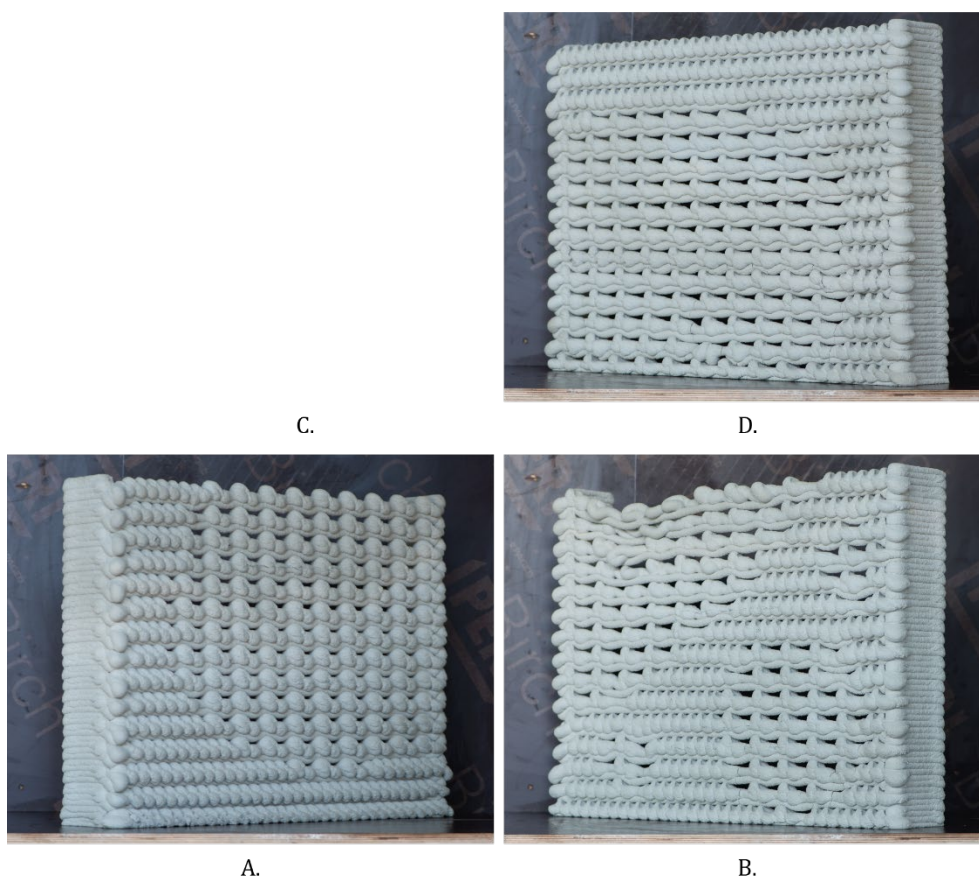


Figure 4.55. individual panels of the multi-panel design, panel C did not succeed during the test prints, panel B showed some failure towards the top layers.

**Size.** The new used panel width of 675mm marks a limit value, that has resulted in some cases in deformation or failure. A commonly used modular size for façade panels is 1m35. In this design, the panels are enlarged to approximately half that size, with a width of 675mm. The height remained the same as in previous panels at 500mm. However, during the printing process, certain panels started to exhibit deformation due to their larger size, as seen in Figure 4.56. Additionally, deformation or even collapse occurred when moving the print before it had fully hardened. This issue was not observed in all panels. It appears that the width of a panel with a *Greek Key Pattern* is limited under 675mm. Previously, with a panel width of approximately 500mm, such issues only arose when the panel was moved carelessly before hardening. To address this problem and print larger panels, a potential solution is to transition from vertical printing on a horizontal print bed to vertical printing on a tilted print bed. This approach would provide support to the print, as it slightly leans against the bed. Figure 4.57 illustrates a schematic example of this setup. However, no tests with a tilted print bed have been conducted, as this requires multiple tests and calibration procedures.



Figure 4.57. Deformation in the panel, caused by to large panel width.

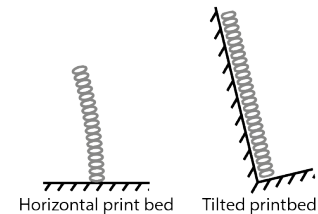


Figure 4.56. Using a tilted print bed gives support to the printed panels, avoiding it to deform.

**Vertical panel connection.** At TU Graz, a technique is employed to achieve a seamless connection between two stacked panels. This involves printing the last few layers of the bottom panel, placing a plastic cover over these layers, and then printing the top panel on top of it. This method ensures a perfect fit between two panels, as it leaves an imprint of the lowest panel in the initial layer. However, this technique proved unsuccessful when applied to panels with a *Greek Key Pattern* in this phase. Two attempts were made, and in both cases, the panels collapsed just before completion. The exact reason for this failure is unclear, but it is likely attributed to a reduced grip on the bottom because of the plastic cover and the large panel width that had already proven to be a limit value. No tests have been conducted however with smaller panel dimensions, so it remains uncertain if this technique would be viable with reduced dimensions.



Figure 4.58. A plastic foil on top of the last lines of the previous panel is used to leave an imprint in the new printed panel.

Consequently, the panels are now printed without using this technique, resulting in a completely flat bottom surface for each panel. The top of the previous panel has a rounded top surface. As a result, there will be a visible seam between the panels.

**Cracking.** Proper treatment of the panels after printing is crucial to minimize cracking. The panels can be covered with a plastic foil, as described in section 4.1.1 (“Horizontal printing”). Cracking is a phenomenon that can happen as the concrete hardens. However, some panels did not get covered immediately with the plastic foil, which has led to cracking. A close-up on such cracks in the panels is provided in Figure 4.59. On the other hand, panels that were covered with the plastic foil promptly after printing showed no signs of cracking. Therefore, it is essential to



Figure 4.59. Panel was not covered with a plastic foil during the hardening process, which has led to cracking.

consistently apply the appropriate treatment to the concrete to prevent cracking.

**Cumulative error.** A small error can cause a cumulative effect of errors, ultimately leading to failure of the panels. This effect was observed in the panel “B.” of the current design. The issue arose from a poor transition between the *Greek Key Shapes* inside and outside the ovals, as shown in Figure 4.60. Specifically, a c.t.c. distance of 59mm was used between two *Greek Keys* on the sixth *Greek Key Layer*. This distance proved to be too large, resulting in significant sagging of the bridging in the next layer. Therefore, the *Greek Keys* printed on top of this sagging exhibited small errors, appearing lower than the rest of the design. This error then propagates to the subsequent layers, magnifying the problem and eventually causing the *Greek Key Shapes* to collapse. Therefore, it is important to carefully consider all the *Greek Keys* in a design to avoid such issues. The same issue arose for panel “C.”, which unfortunately led to collapsed panels as result.

Due to the encountered problems during the printing of the multi-panel design, not all panels had a successful result. Therefore, the panels did not fit together, due to which no global result can be given. With less deformation, the panels should be able to fit together, creating patterns and figures with the perforations.

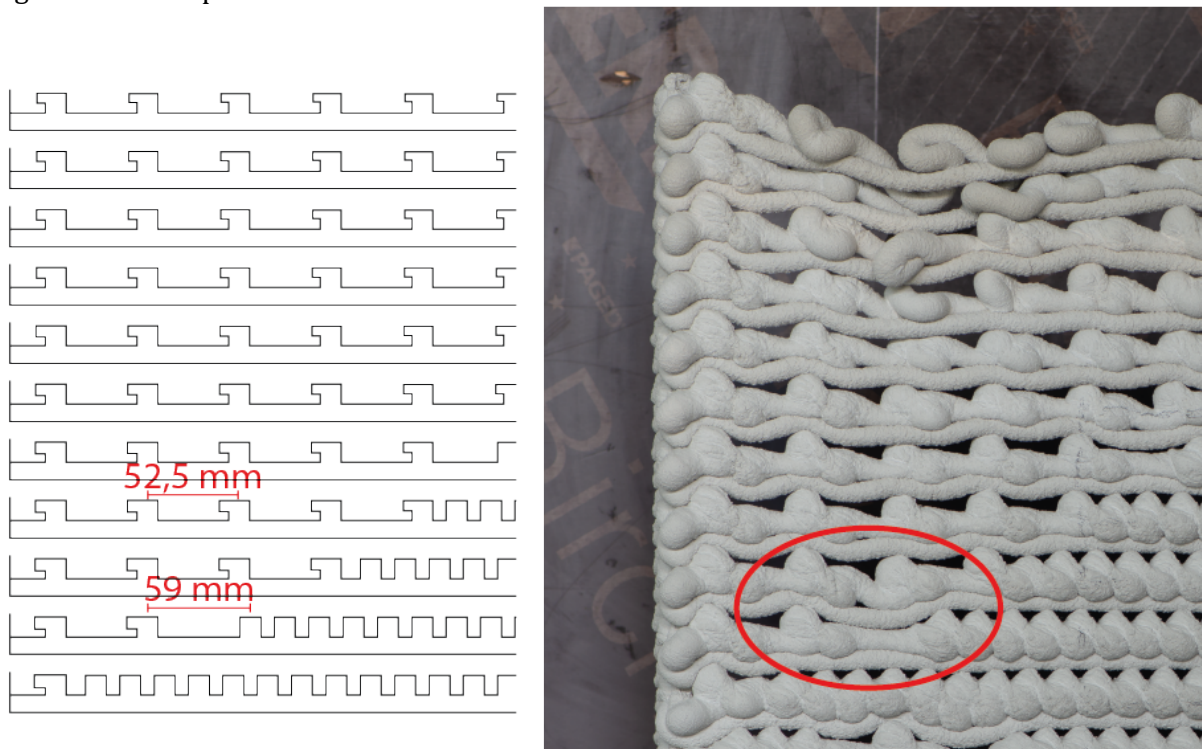


Figure 4.60. A small error leads to failure of the whole panel in a cumulative way.

#### 4.4.2 Closed surface

So far, the printed panels formed a straight square. However, it is also possible to fabricate curved surfaces. A final test print focused on constructing a closed cylinder-shaped surface with the *Greek Key Pattern*. A *Rhino Grasshopper* algorithm generated the toolpath for this surface based on a numerical code. Where each number represented a specific layer. “12131” is the pattern that was repeated to form this cylinder. “1” denoted a straight layer, “2” represented a *Greek Key Layer* with a real height of 35mm, a height ratio of 20%, width of 12mm, an overhang of 5mm and a c.t.c. distance of 25mm. Number “3” on the other hand, indicated a *Greek Key Layer* with a real height of 18mm, a height ratio of 20%, an overhang of 10mm and a width of 12mm. This sequence of

layers was repeated multiple times. By adjusting the input number code, a new order of layers can easily be defined.

With the panels no longer confined to straight shapes, more possibilities arise for utilizing the *Greek Key Pattern*. It can be used to fabricate curved façade panels, but also fabricate interior design elements or other applications. For example, the presented cylinder, was sometimes recognized as a flowerpot. Additionally, a curved surface eliminates the need for side support, as the inherent stability of the shape ensures more structural stability.

**Seam.** At the end of each layer, the printer must move up one layer and print the next layer. For a closed surface, like the cylinder, this movement will show a visible line across the layers. This line is called the seam. This seam is a discontinuity on the surface, that preferably should be as discrete as possible. Figure 4.61 shows the created seam on the presented cylinder surface.



*Figure 4.61.* A seam is visible on a closed surface because the printer moves up from one layer to the next.

## 5. DISCUSSION

### 5.1 Perforations with the *Greek Key*

When deviating from the conventional horizontal movements in 3D concrete printing and incorporating vertical movements, new patterns emerge within this technology. The *Greek Key Pattern* incorporates these vertical movements. Conducted test have proven that by following this toolpath with the 3D concrete printer, perforations are fabricated. Traditional creation of concrete perforated panels requires complex castings. By introducing this new method, a perforated concrete panel can be fabricated, without the need for castings. This will result in less waste material, compared to other construction methods for a perforated concrete façade.

The *Greek Key Pattern and panels* are characterized by ten different parameters that influence their functionality and shape. An overview of the different parameters are listed in Table 5.1, as well as a designated range. It is important to note that these parameter ranges were derived from test prints conducted using the printer setup at *TU Graz*. Different print setups may necessitate adjustments to these parameter ranges. The tests conducted in this research have revealed that certain parameters are correlated with others, thereby affecting the achievable range. For example, a decreasing overhang will result in a lower range for the toolpath height. An increasing toolpath height will result in a decreasing maximum value for the width.

A small error can propagate to subsequent layers and magnify the issue, potentially leading to panel failure. To ensure the quality of the panels and the *Greek Key Pattern*, it is crucial to correctly apply these parameters to ensure no failure occurs in the *Greek Key Geometry*.

Table 5.1. Parameters to describe a *Greek Key Shape/Panel* and the range these parameters must be in.

	<i>Parameter</i>	<i>Unit</i>	<i>Range</i>	<i>Notes</i>
<i>Greek Key parameter</i>	Width	[mm]	0 - 40	Overhang and toolpath height can significantly influence the max width value before collapsing.
	Overhang	[mm]	0 - 25	Larger overhang gives more stability to the <i>Greek Key</i> .
	Toolpath height	[mm]	16 - 35	The maximum toolpath height is in function of the <i>Greek Key width and overhang</i> .
	Height ratio	[%]	10 - 100	/
	Z-height	[mm]	8-12	In ideal circumstances, the Z-height should be 12mm, However, to cope with irregularities from the <i>Greek Key</i> on previous layers, 10mm is a more suitable value.
<i>Panel parameter</i>	Beginpoint	[x,y,z]	/	/
	Centre to centre distance	[mm]	20 - 53	/
	Pattern	[ ]	Regular Alternating	/
	Panel width	[mm]	< 675	For a curved panel, this value can be

Panel Height	[mm]	< 500	The panel height is in relation with the panel width. For a larger width, the height will be more limited.
--------------	------	-------	--

To define the *Greek Key Geometry* in the *Rhino Grasshopper* scripts, a small Python code (Figure 4.41) based on the above-mentioned parameters is used. This code serves as the basis for creating all the panels in the previous phases of the research.

It is concluded that the shape of the *Greek Key* does not significantly impact the appearance of the panels. Variations in the perforations and patterns in the panels are mainly achieved by controlling three parameters: the layer heights, the c.t.c. distance, and the defined pattern of the *Greek Keys*. However, Section 4.2 (“Phase 2: How to control the *Greek Key* with different parameters?”) focuses on controlling the shape of the *Greek Key*, which can vary between a round shape and a moon shape. This analysis has helped to explore the possibilities of the *Greek Key Shapes*, and the associated influence of the parameters on how to control these.

The printed result of the printer shows inconsistencies with the toolpath. No clear resemblance with the toolpath is fabricated. While the toolpath follows the pattern of a *Greek Key*, the printed result fabricates small knots (cfr. The *Greek Keys*) on a printed line, a second straight line is printed on top, bridging between two knots, thereby creating the perforations. A visual comparison between the toolpath and the physical outcome is given in Figure 4.45. Consequently, understanding the shape of the *Greek Key* and how to control it is crucial.

For larger toolpath heights, there is an increased uncertainty in the physical height of the *Greek Keys*, while the smaller toolpath heights show more consistency. A height formula can be used to derive an estimation of the physical height of a single *Greek Key*.

Due to this uncertainty in the height of the *Greek Key*, the subsequent layer may not be adjusted accordingly to this height, due to which it will not be pressed enough into this layer, resulting in insufficient intermixing of the concrete. This will lead to cold joints, that can be prone to breaking under stress.

The outcome of this research is dependent on the used print setup. In this study, the tests were conducted at the processing robot facility from the *ITE* at *TU Graz*. Working with a different robot, print nozzle can drastically influence the shape and size of the extruded line, influencing the final outcome. Also, the used concrete mix can show specific material properties that can lead to different results. Most 3D concrete printer systems prescribe a specific optimized concrete mix for printing. Less viscous material will not be able to perform the needed bridging. The print setup at *TU Graz* employs a two-component system, where an accelerator is added inside the print nozzle to facilitate immediate hardening of the extruded concrete. It is uncertain whether a single-component system, without the accelerator mixture, can achieve the bridging effect required to fabricate the perforation with the *Greek Key Pattern*.

After a panel is printed with the *Greek Key Pattern*, proper treatment of the panel is needed. This can be covered with a plastic foil to avoid cracking during the hardening process. In addition, abrupt movements of the panel must be minimized to prevent displacement. After approximately one day, the concrete has hardened sufficiently to allow movement and lifting of the panel, while full hardening takes about 28 days.

## 5.2 Using the *Greek Key*

While the potential of concrete printing is expanding rapidly, there is limited literature available on the creation of perforations using this novel technology. This research introduces a new technique utilizing a 3D concrete printer to fabricate perforations, broadening the research on this topic.

Perforated façade panels have been printed along this research demonstrating the proposed objectives. A rough surface texture is generated using the *Greek Key Pattern*, by the downward movement of the *Greek Key*, resulting in excessive material pushed sideways falling down on the previous layer. Variations can be made in the size of the perforations. With the toolpath height parameter, the height of the perforations can be controlled while the c.t.c. distance parameter influences the width of the perforations.

The amount of daylight passing through the panel can be calculated using equation 4.9, which corresponds to the perforation ratio of the panel. This ratio can range between 0% up to approximately 20%, depending on the chosen layer heights and c.t.c. distance. The perforated panels produced through this technique are primarily intended for use as façade panels. In a simplified scenario, where light reflection is not calculated, the perforation ratio also functions as an indication for transmitted light. This allows for 0-20% of natural lighting to penetrate the façade. This way, privacy boundaries are maintained, while daylight can penetrate the façade, limiting the need for artificial lighting. Figure 5.1 shows how a light source behind the panels can be perceived.

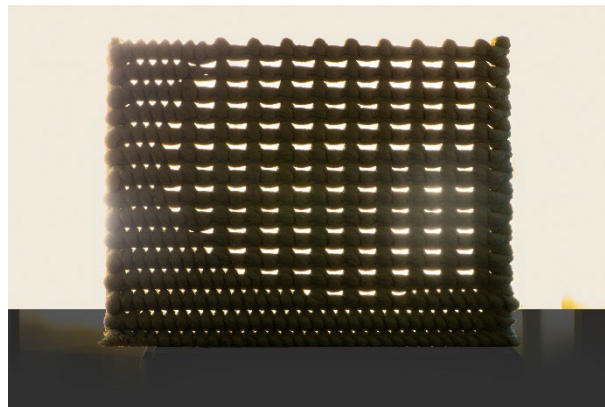


Figure 5.1. A light behind the panel clearly shows the perforations and the pattern of the panels.

This newly developed technique for creating perforations offers several new possibilities and advantages. In alignment with the advantages of 3D concrete printing, the use of the concrete printer offers a construction method with no need for castings and thus less the production of less waste material. Once the design process is complete, the production process is largely automated. This means that no workers have to come close to the robot during printing, creating a safe working environment. With the knowledge gained from this research, panels with different shapes and variations can be fabricated. Additionally, the printing process itself is relatively fast. The panels produced during this research took approximately between five to twenty minutes, depending on the panel size and the created pattern with the perforations.

However, this technique also has its limitations. The size of the panels is restricted, too large panels are designated to show deformations. Although it is possible to combine multiple smaller panels to form larger designs. Even small errors in design or printing can result in cold joints or failure. Furthermore, the strength of the panels is limited due to limited contact points between

layers. Failed panels have been broken in pieces by hand. This showed not much resistance. No tests, however, have been conducted to determine the effective mechanical strength of the panels.

To ensure the precise printing of straight panels, side support is crucial in maintaining their upright position during and after printing. This side support can be created in a traditional layered build-up. However, this will show clear joints in between panels, as the panels show brusque sides. A provided potential solution proposed in this thesis is to print the panels slightly tilted, to avoid the need for support structures.

### 5.3 Further research and improvements

While this research provides an important initial approach to creating and controlling perforations with a 3D concrete printer using the *Greek Key Pattern*, the potential for further exploration in this field is vast. Although many aspects of the *Greek Key* have already been described, there are still numerous approaches to broaden research in this field.

Printing the panels on a tilted print bed, will allow the panels to lean slightly against the print bed and eliminating the need for additional support structures. This has not been tested in this study since significant calibration work and test printing would be required to ensure optimal performance. Transitioning between a flat print bed and a tilted print bed is no evident process, as it necessitates recalibration of the printer environment and precise adjustment of the print bed's location in the Grasshopper files. While this technique holds potential, further research and development are necessary to effectively implement and optimize printing on a tilted print bed.

Currently, the panels printed in this study consisted entirely of the *Greek Key Pattern*. However, further research might evaluate the possibility of combining the *Greek Key* with the traditional layered build-up approach of 3D concrete printing. This exploration could involve incorporating this combination within a single layer or stacking multiple varying layers. The side support is already based on this traditional layered build-up. This hints on the possibility to combine these two techniques. Such integration would open up even more design possibilities with the *Greek Key Pattern*.

In traditional concrete constructions, reinforcement is commonly implemented to avoid failure after cracking. Previous research at the *Institute of Structural design* at *TU Graz* has examined the feasibility of inserting reinforcement along with the extruded concrete in the concrete printer. A special nozzle is used for this. Further steps in the research of the *Greek Key* could involve assessing the possibility of inserting a reinforcement inside the *Greek Keys*. This could help prevent the initial cracking of the concrete.

To expand the application of the *Greek Key*, it is essential to test the *Greek Key Pattern* on different print setups as well. Successful fabrication of perforations from such further research can broaden the application of the *Greek Key Pattern*, making it accessible to architects and designers with access to a 3D concrete printer.

The scale of the *Greek Key Pattern* is defined based on the print setup at *TU Graz*. By working with a different print setup, potentially, a different scale can be applied. Using a larger nozzle, for example, can lead to thicker panels with enhanced structural integrity, potentially allowing for larger panel dimensions. Conversely, using a smaller nozzle can enable the creation of finer perforations and textures. This raises the question of whether the *Greek Key Pattern* is applicable with different materials, such as with 3D clay printing. Exploring different scales and materials can open up new possibilities in line with this research.

The disparity between the digital input and the physical outcome of the *Greek Key* cause that no resembling 3D model can be designed for visualization prior to printing. Consequently, architects and designers face limitation in presenting their designs incorporating the *Greek Key*. They are not able to generate renders or incorporate these complex shapes into presentation documents. To address this issue, a digital module can be developed to accurately predict the output of the 3D concrete printer and generate a representative 3D model. This module should take into account the material's viscosity, gravitational forces, and the printer's interactions. By incorporating these factors, the generated model will more effectively reflect the final printed result, enabling architects and designers to effectively communicate and visualize their designs.

This research has mostly focused on creating individual panels for fictional designs. No panels have been installed yet. It is crucial to define a functional installation method to effectively utilize the panels in a realistic setting. This could involve using anchors, an external frame or incorporating a hollow side support system in which tensioning can be inserted across multiple panels. Further research can explore these possibilities and determine the most functional installation method.

By addressing these future research directions, the understanding and application of the *Greek Key Pattern* can be significantly advanced. The outcomes of such investigations will have implications for the broader adoption of 3D concrete printing, more specifically the *Greek Key Pattern*, in various industries.

## 6. CONCLUSION

The *Greek Key Pattern* defines a contribution to the field of 3D concrete printing. Leveraging the capabilities of the parametric design software *Rhino Grasshopper*, the geometry of the *Greek Key* can be accurately scripted, enabling the generation of perforations in a new form language. The *Rhino Grasshopper* script utilizes a set of parameters that define both the individual *Greek Key Shape* and the panel constructed by the *Greek Key Pattern*. To define an individual *Greek Key Shape*, this involves five different parameters, including: “Width”, “Overhang”, “Toolpath height”, “Height ratio” and “Z-height”; To define the *Greek Key Panel*, five other parameters are used: “Begin point”, “C.t.c. distance”, “Pattern”, “Panel width” and “Panel Height”. These parameters provide control over the perforation’s characteristics, and over the overall shape of the panels.

This research deviates from the conventional horizontal layer-by-layer approach by introducing vertical movement from the *Greek Key* into the print. This allows for the creation of controlled perforations. A notable outcome of this research is the observed discrepancy between the toolpath geometry and the physical outcome. Despite this irregularity, the *Greek Key Pattern* successfully demonstrated the ability to generate controlled perforations. Adjusting the “toolpath height” and the “c.t.c. distance” parameters provided control over the size and spacing of the perforations.

The resulting panels showcased the intended variations in perforation size and exhibited a desirable rough surface texture, achieved through the displacement of excess material during the downward movement of the 3D concrete printer at the end of the *Greek Key Geometry*.

It is important to acknowledge that each defined *Greek Key* exhibited slight differences due to the characteristic of the freshly extruded concrete, resulting in a small degree of uncertainty in the design of a *Greek Key Pattern*. However, these variations did not compromise the integrity of the panels. Furthermore, the research identified the potential for estimating the real height of a *Greek Key Shape*, contributing to a better understanding of the printing process and its outcomes.

Moving forward, future research might focus on creating practical applications with this new form language, including the development of installation methods for these perforated panels, as this research was limited to fictional designs, with no installation method yet presented. Additionally, to expand the scope of this research to different hardware setups would enhance the applicability of the *Greek Key Pattern*, increasing accessibility to the *Greek Key Pattern*.

The findings presented in this study have enriched the field of 3D concrete printing by introducing a new form language and providing valuable insights into the creation and control of perforations using a 3D concrete printer. This research has successfully addressed the main research question of creating and controlling perforations with a 3D concrete printer, by successfully demonstrating the creation of perforations using the *Greek Key Pattern*. The objectives of creating a new form language, achieving perforated panels with varying characteristics, in combination with a rough surface texture have been accomplished.

By introducing the *Greek Key Pattern* for 3D concrete printing and by establishing a foundation for future studies, this research contributes to the advancement of 3D concrete printing techniques and offers architects and designers new possibilities for innovative and customizable perforated façade panels.

## 7. BIBLIOGRAPHY

- 3D Potter. (n.d.). *Continuous Flow High Volume Pump Overview*. 3D Potter. Retrieved June 4, 2023, from <https://3dpotter.com/continuous-flow-high-volume-pumps>
- ABB. (2004). *Technical reference manual RAPID Instructions, Functions and Data types*.
- ABB. (2020). *IRB 6660 Product specification*.  
<https://search.abb.com/library/Download.aspx?DocumentID=3HAC028207-001&LanguageCode=en&DocumentPartId=&Action=Launch>
- Addanki, S., Amiri, I. S., & Yupapin, P. (2018). Review of optical fibers-introduction and applications in fiber lasers. *Results in Physics, 10*, 743–750.  
<https://doi.org/https://doi.org/10.1016/j.rinp.2018.07.028>
- Bekkering Adams Architecten. (2017). *Firewall*. Studio Adams.  
<https://www.studioadams.nl/projects/69/firewall>
- Bekkering, J., Kuit, B., Biffi, A., & Ahmed, Z. Y. (2020). Architectonic Explorations of the Possibilities of 3D Concrete Printing: The Historic Building Fragment as Inspiration for New Applications with 3D Concrete Printing in Architecture. In F. P. Bos, S. S. Lucas, R. J. M. Wolfs, & T. A. M. Salet (Eds.), *Second RILEM International Conference on Concrete and Digital Fabrication* (pp. 1078–1090). Springer International Publishing.
- Berman, B. (2012). 3-D printing: The new industrial revolution. *Business Horizons, 55*(2), 155–162. <https://doi.org/https://doi.org/10.1016/j.bushor.2011.11.003>
- Bernier, C. (2021, November 10). *Six-Axis Robots: Applications, Benefits, and Cost Analysis*. #HowToRobot. <https://howtorobot.com/expert-insight/six-axis-robots>
- Bhushan, M. P., Johnson, D., Pasha, M. A. B., & Prasanthi, K. (2013). Optical fibres in the modeling of translucent concrete blocks. *International Journal of Engineering Research and Applications, 3*(3), 13–17.
- Chen, S. (2019, July 11). *Can Robots Solve the Affordable Housing Crisis?*. PoliticoMagazine. <https://www.politico.com/magazine/story/2019/07/11/robots-solve-affordable-housing-crisis-227276/>
- Chi, P., & Doris, A. (2019). A Comprehensive Evaluation of Perforated Façades for Daylighting and Solar Shading Performance: Effects of Matrix, Thickness and Separation Distance. *Journal of Daylighting, 6*(2), 97–111. <https://doi.org/10.15627/jd.2019.10>
- Claire Im, H., Alothman, S., & García del Castillo, J. L. (2018). *Responsive Spatial Print. Clay 3D printing of spatial lattices using real-time model recalibration*. 286–293.  
<https://doi.org/10.52842/conf.acadia.2018.286>
- Constructions-3D. (n.d.). *Maxi Printer*. Aniwaa. Retrieved March 3, 2023, from <https://www.aniwaa.fr/produit/imprimantes-3d/machines-3d-3d-constructeur/>
- Costantino, D., Grimaldi, A., & Pepe, M. (2022). 3D modelling of buildings and urban areas using grasshopper and rhinoceros. *Geographia Technica, 17*(1/2022), 167–176.  
[https://doi.org/10.21163/GT\\_2022.171.13](https://doi.org/10.21163/GT_2022.171.13)

- Cybe Construction. (2018). *3D concrete printers*. <https://cybe.eu/3d-concrete-printing/printers/>
- Dreamstime. (n.d.). *Seamless stone border stock image*. Dreamstime. Retrieved March 12, 2023, from <https://www.dreamstime.com/seamless-stone-border-greek-style-ancient-marble-mosaic-texture-background-material-library-d-renders-seamless-stone-image210465769>
- Egonis. (n.d.). *LiTraCon – przezierny beton*. Architektura Dla Każdego. Retrieved July 6, 2022, from <http://architekturadlakazdego.blogspot.com/2011/05/litracon-przezierny-beton.html>
- Ghasemishkaftaki, M., A Ortiz, M., & Bluysen, P. (2021). An overview of transparent and translucent 3D-printed façade prototypes and technologies. *Paper Presented at Healthy Buildings Europe 2021 Online*.
- GRZ Software. (n.d.). *Toolpath*. Retrieved November 23, 2023, from <https://www.grzsoftware.com/learn-cnc/terms/toolpath/>
- Hull, C. W. (2015). The Birth of 3D Printing. *Research-Technology Management*, 58(6), 25–30. <https://doi.org/10.5437/08956308X5806067>
- Institute of Structural Design. (n.d.). *Robotics Design Laboratory*. TU Graz. Retrieved March 13, 2023, from <https://www.tugraz.at/en/institutes/ite/robotics-design-laboratory/>
- Kim, J., Jung, J., Kim, S., & Kim, S.-A. (2017). Multi-Factor Optimization Method through Machine Learning in Building Envelope Design: Focusing on Perforated Metal Façade. *International Journal of Architectural and Environmental Engineering*, 11(11), 1602–1609.
- Knuff, A. (2017). *Pattern Research Project: An Investigation of The Pattern And Printing Process - Greek Key* (Pattern Research Project).
- Ko, C.-H. (2021). Constraints and limitations of concrete 3D printing in architecture. *Journal of Engineering, Design and Technology*, 20(5), 1334–1348. <https://doi.org/10.1108/JEDT-11-2020-0456>
- Kosky, P., Balmer, R., Keat, W., & Wise, G. (2021). Manufacturing Engineering. In P. Kosky, R. Balmer, W. Keat, & G. Wise (Eds.), *Exploring Engineering* (5th ed., pp. 259–291). Academic Press. <https://doi.org/https://doi.org/10.1016/B978-0-12-815073-3.00012-0>
- Malaeb, Z., AlSakka, F., & Hamzeh, F. (2019). 3D Concrete Printing: Machine Design, Mix Proportioning, and Mix Comparison Between Different Machine Setups. In J. G. Sanjayan, A. Nazari, & B. Nematollahi (Eds.), *3D Concrete Printing Technology* (pp. 115–136). Butterworth-Heinemann. <https://doi.org/https://doi.org/10.1016/B978-0-12-815481-6.00006-3>
- Mendonça, P., & Macieira, M. R. F. (2019). Architectural Membranes for improving the functional performance of buildings. *SMC Magazine*, 3, 27–38.
- Oxford Languages. (n.d.). *3D printing*. Retrieved November 19, 2022, from <https://www.google.com/search?q=3D+printing+define&oq=3D+printing+define&aqs=chrome.69i59j0i512l9.2559j0j7&sourceid=chrome&ie=UTF-8>
- Paoletti, I. (2017). Mass Customization with Additive Manufacturing: New Perspectives for Multi Performative Building Components in Architecture. *Procedia Engineering*, 180, 1150–1159. <https://doi.org/https://doi.org/10.1016/j.proeng.2017.04.275>

- Ranveer, A., Bhanuse, M., & Babar, A. (2016). Smart Light Translucent Concrete By Using Optical Fiber. *Journal of Environmental Science, Computer Science and Engineering & Technology*, 5, 10–18.
- Raspall, F. (2013). *Faksimile / Big scale. [Course text]*.
- Rhino Grasshopper (1.0.0007). (2022). Robert McNeel & Associates.
- Robert McNeel & Associates. (n.d.). *Rhinoceros Forums*.  
<https://discourse.mcneel.com/c/grasshopper/2>
- Robert McNeel & Associates. (n.d.). *About McNeel*. Retrieved May 30, 2023, from  
<https://www.rhino3d.com/mcneel/about/>
- Romaniak, K., & Filipowski, S. (2018). Parametric design in the education of architecture students. *World Transactions on Engineering and Technology Education*, 16, 386–391.
- Rusi, I. (2019). The Contemporary Trend of Perforation. Case of Exoskeleton Concrete Shells. *International Journal of Science and Research (IJSR)*, 8.
- Sarakinioti, M.-V., Konstantinou, Thaleia, Turrin, M., Tenpierik, M., Loonen, R., de Klijin-Chevealerias, M., & Knaack, U. (2018). Development and prototyping of an integrated 3D-printed façade for thermal regulation in complex geometries. *Journal of Facade Design and Engineering*, 6(2), 29–40.
- Schmidt, M., & Slowik, V. (2009). *Capillary shrinkage cracking and its prevention by controlled concrete curing*.
- Stevenson, K. (2021, August 24). *Diamond Age's Advanced Construction 3D Printing Concept*. Fabbaloo. <https://www.fabbaloo.com/news/diamond-ages-advanced-construction-3d-printing-concept>
- Strauß, H., & Knaack, U. (2016). Additive Manufacturing for Future Facades: The potential of 3D printed parts for the building envelope. *Journal of Facade Design and Engineering*, 3, 225–235. <https://doi.org/10.3233/FDE-150042>
- Strieder, J. (2005). Why Add Accelerating Admixtures to Concrete. *Concrete Decor*, 5(5).
- StudioAdams. (2017). *Firewall*. <https://www.studioadams.nl/projects/69/firewall>
- Teague, L. (2017, January 31). 3D printing is making an impression on concrete. *Frame*.  
<https://www.frameweb.com/article/3d-printing/3d-printing-is-making-an-impression-on-concrete>
- Tissink, A. (2017, February 6). Beton als Viennetta. *Cobouw*, 24–27.  
<https://www.studioadams.nl/downloads/modules/publications/Bekkering%20Adams%20Architects-Cobouw%20article-Beton%20als%20viennetta-170216.pdf>
- V., C. (2020, April 8). *Rhino: what are the features of this 3D modeling software*. 3Dnatives.  
<https://www.3dnatives.com/en/rhino-3d-modeling-software-080420205/>
- Wangler, T., Lloret, E., Reiter, L., Hack, N., Gramazio, F., Kohler, M., Bernhard, M., Dillenburger, B., Buchli, J., Roussel, N., & Flatt, R. (2016). Digital Concrete: Opportunities and Challenges. *RILEM Technical Letters*, 1, 67–75. <https://doi.org/10.21809/rilemtechlett.2016.16>
- Wasp. (n.d.). *Delta WASP 3MT CONCRETE*. Wasp. Retrieved March 3, 2023, from  
<https://www.3dwasp.com/en/concrete-3d-printer-delta-wasp-3mt-concrete/>

- Xu, M., David, J. M., & Kim, S. H. (2018). The Fourth Industrial Revolution: Opportunities and Challenges. *International Journal of Financial Research*, 9(2), 90–95.  
<https://doi.org/10.5430/ijfr.v9n2p90>
- Zant, P., Roosendaal, D., & Van Dongen, J. (2023). *Printer options: match your strategy with your printer. [Webinar]*. CYBE. <https://cybe.eu/webinars/webinar-printer-options/>
- Zhang, X., & Liou, F. (2021). Introduction to additive manufacturing. In J. Pou, A. Riveiro, & J. P. Davim (Eds.), *Additive Manufacturing* (pp. 1–31). Elsevier.  
<https://doi.org/https://doi.org/10.1016/B978-0-12-818411-0.00009-4>
- Zielińska, M., & Ciesielski, A. (2017). Analysis of Transparent Concrete as an Innovative Material Used in Civil Engineering. *IOP Conference Series: Materials Science and Engineering*, 245(2), 022071. <https://doi.org/10.1088/1757-899X/245/2/022071>